ANL-ARC-250

Sodium Pool Fire Phenomena, Sodium Pool Fire Modeling in SOFIRE II, and SOFIRE II Calculations for the AFR-100

Nuclear Engineering Division

About Argonne National Laboratory

Argonne is a U.S. Department of Energy laboratory managed by UChicago Argonne, LLC under contract DE-AC02-06CH11357. The Laboratory's main facility is outside Chicago, at 9700 South Cass Avenue, Argonne, Illinois 60439. For information about Argonne, see http://www.anl.gov.

Availability of This Report

This report is available, at no cost, at http://www.osti.gov/bridge. It is also available on paper to the U.S. Department of Energy and its contractors, for a processing fee, from:

U.S. Department of Energy
Office of Scientific and Technical Information
P.O. Box 62
Oak Ridge, TN 37831-0062
phone (865) 576-8401
fax (865) 576-5728
reports@adonis.osti.gov

Disclaimer

This report was prepared as an account of work sponsored by an agency of the United States Government. Neither the United States Government nor any agency thereof, nor UChicago Argonne, LLC, nor any of their employees or officers, makes any warranty, express or implied, or assumes any legal liability or responsibility for the accuracy, completeness, or usefulness of any information, apparatus, product, or process disclosed, or represents that its use would not infringe privately owned rights. Reference herein to any specific commercial product, process, or service by trade name, trademark, manufacturer, or otherwise, does not necessarily constitute or imply its endorsement, recommendation, or favoring by the United States Government or any agency thereof. The views and opinions of document authors expressed herein do not necessarily state or reflect those of the United States Government or any agency thereof, Argonne National Laboratory, or UChicago Argonne, LLC.

ANL-ARC-250

Sodium Pool Fire Phenomena, Sodium Pool Fire Modeling in SOFIRE II, and SOFIRE II Calculations for the AFR-100

prepared by
James J. Sienicki and Anton Moisseytsev
Nuclear Engineering Division, Argonne National Laboratory

September 24, 2012

Abstract

The SOFIRE II computer code for the calculation of sodium pool fires has been obtained from the Reactor Safety Information Computational Center and the SOFIRE II ONE CELL version has been implemented at Argonne National Laboratory (ANL). A critical review of literature relevant to sodium pool fires has been carried out with the objectives of understanding sodium pool fire phenomena and how well specific phenomena are modeled or neglected in SOFIRE II. Significant predictions about sodium pool fires can be made on the basis of first principles analyses alone making use of the existing experiment database and knowledge base. In implementing SOFIRE II ONE CELL, minor modifications were necessary to compile and execute the code on a personal computer (PC) and to verify the results of the test case problem. The code was applied to the AFR-100 Sodium-Cooled Fast Reactor (SFR) design to calculate a sodium pool fire following a postulated failure of the sodium storage vessel of one of the four intermediate sodium heat transport circuits and the subsequent release of sodium onto the floor of the steel-lined compartment in which the sodium storage vessel is located. SOFIRE II calculates that only a small fraction of the released sodium burns due to the rapid consumption of the available oxygen inside of the closed compartment. The preliminary results demonstrate the effects of the heat sinks provided by the compartment floor, walls, and ceiling in reducing the temperature of the sodium pool with time.

Table of Contents

LIST OF FIGURES

LIST OF TABLES

1 Introduction

The SOFIRE II code for the analysis of sodium pool fires is an older computer code and hasn't undergone any further development in the U.S. since it was partially documented in the User Manual in 1973 [1]. Significant experiment and analysis work on sodium pool fires was subsequently carried out and an extensive understanding of sodium pool fires and their potential consequences has been developed. The articles by Newman [2 through 5] provide a good summary of much of what is known about sodium pool fires. The following discusses the phenomena relevant to sodium pool fires and indicates how those phenomena are modeled in SOFIRE II or are neglected in SOFIRE II. Some noteworthy previous extensions of SOFIRE II in Japan and India are also discussed.

2 Sodium Pool Burning Phenomena and SOFIRE II

2.1 Sodium Pool Burning Phenomena and Pool Burning Rates

When a component or pipe fails, sodium is initially released as a stream having a configuration and diameter reflecting the configuration and size of the break over a time dependent upon sodium flow through the break. Depending upon the circumstances, the stream may partially or completely break up into droplets giving rise to a sodium spray fire in the presence of an oxidizer such as the oxygen in air. The stream may impact upon other components or piping resulting in further breakup. Sodium collects upon the floor forming a pool that burns. SOFIRE II only treats burning of a sodium pool and ignores any other sodium burning modes; the sodium pool is assumed to be formed instantly.

The lowest partial pressure of oxygen for ignition of sodium is reported to have been 3 % [5]. For a pool configuration, ignition temperatures of 300 to 320 °C are reported in damp atmospheres, 200 °C in dry air/oxygen, and as low as 120 to 150 °C if the sodium is stirred or in the form of drops such that surface layers are broken up [5].

It is well established that the rate of burning of a sodium pool is limited by the rate of oxygen transport to the pool upper surface. The burning rate can thus be formulated in terms of a mass transfer coefficient times the air density times the difference between the bulk oxygen weight fraction and the oxygen weight fraction at the flame zone (i.e., zero). This was understood before 1973 and is thus incorporated into SOFIRE II. The SOFIRE II code assumes a mass transfer coefficient obtained from a heat transfer coefficient for turbulent natural convection from a horizontal flat plate by replacing the Nusselt number by the Sherwood number and the Prandtl number by the Schmidt number. For sodium pools having a diameter/size of about 0.1 m or greater, the flow is turbulent whereas for smaller diameter pools the flow is laminar and a different mass transfer correlation for laminar flow should be used [5].

As a check on the turbulent mass transfer and heat transfer correlations assumed in SOFIRE II, the author is familiar with the correlation of Globe and Dropkin for natural convection in liquids confined between two horizontal plates with heating at the lower plate and cooling at the upper plate [6]. Their Nusselt number correlation is

$$\mathrm{Nu} = 0.069\left(\mathrm{Gr}\,\mathrm{Pr}\right)^{\frac{1}{3}}\mathrm{Pr}^{0.074}$$

where

Nu = Nusselt number,

Gr = Grashof number,

Pr = Prandtl number.

Their correlation spanned Rayleigh numbers, Ra = Gr Pr, from 1.51×10^5 to 6.76×10^8 and Prandtl numbers from 0.02 to 8750.

The Globe and Dropkin experiments incorporated heating at a lower surface and cooling at an upper surface. The Nusselt number thus describes the effects of a resistance to heat transfer at the lower surface and a resistance to heat transfer at the upper surface assuming that the effects of turbulent natural convection result in a more or less uniform temperature distribution across most of the height between the upper and lower plates with the exception of the regions near the plates. Assuming that the resistances are identical because the rate of heating equals the rate of cooling in steady state, the heat transfer coefficient at the lower plate alone is given by the inverse of half of the combined resistance. It follows that the Nusselt number for heat transfer at the lower plate alone is equal to twice that for heat transfer at both plates. Thus, it is expected that the heat transfer correlation for turbulent natural convection from a heated horizontal surface is

$$\mathrm{Nu} = 0.138 \left(\mathrm{Gr}\,\mathrm{Pr}\right)^{\frac{1}{3}} \mathrm{Pr}^{0.074} \quad .$$

The correlation assumed in SOFIRE II is

$$\mathrm{Nu} = 0.14 \left(\mathrm{Gr}\,\mathrm{Pr}\right)^{\frac{1}{3}} \quad .$$

This correlation is for turbulent natural convection from upward facing horizontal plates and is attributed to Fishenden and Saunders [7]; it was commonly used at the time that SOFIRE II was developed.

The Grashof number is proportional to the cube of a length scale which is the height difference between the upper and lower surfaces in the Globe and Dropkin case and the plate length in the case of a correlation for natural convection from a horizontal plate such as the correlation of Fishenden and Saunders. However, because of the 1/3 power dependency of the Nusselt number, the length scale drops out of the equation for the heat transfer coefficient. In calculating natural convection heat transfer off of a burning sodium pool, a question would be what value to use for the length scale which is related to the size of the flame zone above the sodium which is poorly known or the diameter or side length of the pool. The cancellation of the length scale in the heat transfer coefficient is fortuitous enabling the calculation of turbulent natural convection heat transfer per unit area or mass transfer per unit area from a burning pool without needing to know the diameter or side length of the pool.

In SOFIRE II as well as other treatments of oxygen mass transfer to the flame zone, the mass transfer coefficient is obtained by simply replacing the Nusselt number by the Sherwood number and the Prandtl number by the Schmidt number. Thus, the Sherwood number correlation assumed in SOFIRE II is

$$\mathrm{Sh} = 0.14\left(\mathrm{Gr}\,\mathrm{Sc}\right)^{\frac{1}{3}}$$

where

Sh = Sherwood number,

Sc = Schmidt number.

For forced convection flow in which heat transfer depends upon a Reynolds number, Re, and a Prandtl number, replacing Nu by Sh and Pr by Sc is valid because the heat and mass transfer equations are similar; both depend upon the same velocity field that is determined by only the configuration and Re. However, in general, this prescription is incorrect for thermally-driven natural convection because the velocity field depends upon the configuration, the Grashof number, and the Prandtl number. The configuration and Grashof number alone do not determine the velocities in the way that the configuration and Reynolds number do for forced convection. An example is the correlation for natural convection from a vertical flat plate of Churchill and Chu [8]. For the case of a liquid metal such as sodium for which Pr/Sc → 0, the Sherwood number for thermally-dominated natural convection is obtained from the Nusselt number by replacing

$$\mathrm{Ra} = \mathrm{Gr}\,\mathrm{Pr}$$

by

$$\mathrm{Ra}\left(\frac{\mathrm{Sc}}{\mathrm{Pr}}\right)^{\frac{4}{3}}.$$

In contrast, for the case in which the Schmidt and Prandtl numbers are equal, Sc = Pr, Churchill and Chu recommend replacing GrPr by GrPr + Gr'Sc where the latter is a "Rayleigh number," Ra' = Gr'Sc, reflecting the effects of changes in specific volume arising from changes in composition. For example, reaction of oxygen and carbon dioxide with sodium removes oxygen and carbon dioxide from air changing the air density and contributing to natural convection. Their recommendation is based upon earlier results of an investigation by Saville and Churchill [9].

For air at atmospheric pressure and a temperature of 60 °C, the diffusivity of oxygen in nitrogen is 2.74×10^{-5} m^2/s. The thermal diffusivity of air at atmospheric pressure and 60 °C is 2.65×10^{-5} m^2/s. Thus, the diffusivities for mass transfer of oxygen in air and for heat transfer in air are nearly identical. The diffusivity for momentum, μ/ρ, is equal to 1.89×10^{-5} m^2/s. The Prandtl number is defined as the ratio of the diffusivity for momentum to the diffusivity for heat and equals 0.713. The Schmidt number is the ratio of the diffusivity for

momentum to the diffusivity of oxygen in nitrogen and equals 0.690 which is only 3.3 % less than the Prandtl number.

According to the recommendation of Churchill and Chu, one would expect that the mass transfer coefficient is obtained from the heat transfer coefficient by replacing Nu by Sh and GrPr by GrPr + Gr'Sc. The second term is expected to be relatively small compared to the first because the specific volume changes due to removal of oxygen and carbon dioxide from air are small compared to the specific volume changes due to changes in temperature. Thus, the Prandtl number should not be replaced by the Schmidt number in the Sherwood number correlation; the Prandtl number should be retained. However, because the Prandtl and Schmidt numbers are so close, replacing Pr by Sc doesn't produce any significant error. The prescription that has been followed in sodium pool fire analysis of replacing Pr by Sc is incorrect but has worked simply because of the fortunate situation that Pr and Sc for air reacting with sodium are virtually the same.

Al-Arabi and El-Riedy [10] reviewed earlier heat transfer correlations for natural convection from upward facing horizontal plates and performed experiments for natural convection of air from upward facing horizontal plates for Rayleigh numbers, Ra, between 2×10^5 and 10^9. The transition between laminar and turbulent flow was found to occur at a Rayleigh number of about 4×10^7. For the turbulent regime, they obtained the heat transfer correlation,

$$\mathrm{Nu} = 0.155\left(\mathrm{Gr}\,\mathrm{Pr}\right)^{\frac{1}{3}} .$$

Al-Arabi and El-Riedy stated that the uncertainty associated with their correlation is ± 12 %. Their correlation provides Nusselt numbers that are 10.7 % greater than the earlier Fishenden and Saunders correlation assumed in SOFIRE II. Based upon the Al-Arabi and El-Riedy correlation, SOFIRE II might thus underestimate the sodium pool burning rate by 9.68 %.

For the laminar regime, Al-Arabi and El-Riedy obtained the correlation,

$$\mathrm{Nu} = 0.70\left(\mathrm{Gr}\,\mathrm{Pr}\right)^{\frac{1}{4}} ,$$

which they claimed has an uncertainty of ± 14 %.

The Rayleigh number,

$$\mathrm{Ra} = \mathrm{Gr}\,\mathrm{Pr} = \frac{\rho^2 c_P g \beta \Delta T L^3}{\mu k},$$

where

ρ = density,

c_P = specific heat,

g = gravitational acceleration,

β = volume coefficient of thermal expansion,

ΔT = temperature difference between plate surface and bulk atmosphere,

L = plate length,

μ = viscosity,

k = thermal conductivity.

The reaction products of sodium burning with oxygen are sodium oxide, Na_2O, and sodium peroxide, Na_2O_2. Examinations of residues from sodium pool fire experiments have revealed the presence of both sodium oxide and sodium peroxide. SOFIRE II assumes an input constant specifying the fraction of oxygen consumed in producing sodium oxide versus sodium peroxide. This input constant determines the amount of sodium reacted per unit mass of oxygen consumed as well as the heat release per unit mass of oxygen consumed. The constant ratio is assumed throughout the duration of the SOFIRE II calculation. In reality, the amounts of oxide and peroxide created vary over time. This was recognized in 1973 and is even discussed in the User Manual with regard to comparison with data. With the constant input parameter, SOFIRE II has been compared with data inputting the ratio measured posttest and assuming the same input parameter throughout a calculation. Of course, this is not a true test of the code predictions versus experiment as one would have in a blind pretest prediction without knowledge of the relative amounts of oxide and peroxide residues generated during the test beforehand.

According to Newman, sodium burning initiates with flameless combustion involving rapid surface oxidation with the formation of a grey purple product close to the sodium surface. Initially, sodium oxide is formed. The theoretical density of sodium oxide is 2270 kg/m^3 compared with a sodium density of 811 kg/m^3. However, for pool surface temperatures below 600 °C, the sodium oxide accumulates atop the upper surface of the sodium pool. Newman [5] attributes this behavior to the existence of a supporting layer on the surface of the liquid metal sodium associated with the grey purple layer observed during the pool ignition phase. The oxide surface thickness rapidly grows and wrinkles with oxide nodules or pillars growing in random locations. Newman continues to describe how at 350 to 450 °C, small flames marked by light and dark smoke emissions appear on the nodules marking the beginning of vapor phase combustion. The oxide pillars are porous and are recognized to act as wicks into which sodium is drawn upward by capillary action and heated. Because the rate of sodium transport is limited and the sodium becomes remote from the underlying pool, there is an overabundance of oxygen such that further oxidation to sodium peroxide occurs. Sodium peroxide is yellow and can be observed as distinct from white sodium oxide during

burning. Newman notes that at a later stage liquid sodium can begin to wet the oxide and is drawn up to react with peroxide releasing heat as it reduces the peroxide to oxide further contributing to vapor phase combustion [5].

Vapor combustion on the nodules continues until the pool attains a temperature of about 600 °C when the nodules appear to sink into the pool or disappear. Newman associates this transition with wetting or decomposition of the grey layer at about 600 °C such that the overlying wicks are no longer supported upon the grey layer raft [5]. Analysis of the grey layer revealed that carbon is a major constituent presumably formed by the reaction,

$$\frac{4}{3}\mathrm{Na}+\mathrm{CO_2}\rightarrow\frac{1}{3}\mathrm{C}+\frac{2}{3}\mathrm{Na_2CO_3},$$

with atmospheric CO_2. Newman states that calcium, silicon, and oxygen were also detected in the carbon-based compound and that it has been proposed that the compound may disappear due to oxidation of the carbon by traces of Na_2O_2 formed near the carbon layer but not in direct contact with the sodium. The Na_2O_2 could be formed by interactions between Na_2O and O_2 or CO_2 and Na_2CO_3. He also notes that alkali metal oxides and carbonates are known to catalyze the ignition of carbon and lower the ignition temperature to about 600 °C.

Above 600 °C, combustion occurs with a flat flame close to the pool surface. Sodium oxide is formed either by surface reaction or vapor phase reaction, deposits on the pool surface, is wetted by sodium, and sinks into the pool. The oxide accumulates in the pool and as sodium is reacted the upper part of the oxide is exposed while the sodium level falls. Because the sodium inside of the oxide structure is less mobile, the burning rate declines. Newman notes that sodium pool fires rarely burn to completion with a significant amount of unburned sodium remaining. Subsequent reaction of sodium oxide to sodium peroxide on the residues of pool fires have been observed to occur over minutes.

The maximum sodium temperature during burning of an unconfined pool is stated to be about 730 °C which represents a steady state in terms of heat release inside the flame and heat losses from the flame to the pool and from the flame to the surroundings [5]. Of course, this is significantly greater than the sodium temperatures inside of a SFR intermediate sodium loop implying that the sodium pool temperature will rise following a sodium release and pool collection.

In support of the raft layer explanation, Newman describes how below 600 °C the surface nodules could be pushed below the liquid surface in deep pools. However, the sodium oxide nodules/wicks that form are porous. It is speculated here that sodium need not be drawn up by capillary action to fill all of the porosity. If this is the case, then it is possible for the effective density of the oxide to be less than that of the underlying sodium provided that the sodium oxide volume fraction in the nodule/wick layer is low enough. In particular, it is required that

$$\rho_{Na_2O}\,\alpha_{Na_2O}+\rho_{Na}\,\beta_{Na}\,(1-\alpha_{Na_2O})<\rho_{Na}$$

where

α_{Na2O} = sodium oxide volume fraction in oxide nodule/wick,

β_{Na} = fraction of porosity in oxide nodule/wick filled with sodium.

Solving for the sodium oxide volume fraction, the requirement is that

$$\alpha_{Na_2O}<\frac{1-\beta_{Na}}{\frac{\rho_{Na_2O}}{\rho_{Na}}-\beta_{Na}}.$$

At 600 °C, the density ratio is 2.80. If sodium is assumed to occupy only half of the oxide volume, such that β_{Na} = 0.5, then the limiting sodium oxide volume fraction is calculated to equal 0.22. The author has shown that previous data indicates that sodium oxide deposits formed due to precipitation of dissolved oxide in sodium can have very low sodium oxide volume fractions well below this value. Hence, it is possible that the oxide formed during sodium burning is also highly porous and that with incomplete filling by sodium this at least contributes to a lower overlying weight to be supported by the carbon-based raft layer.

Recently reported experiments [11 and 12] show the formation of sodium oxide dendrites during the combustion of individual sodium droplets in nitrogen-oxygen mixtures. In some instances, dendrite growth was driven by precipitation of dissolved oxygen from the interior of the sodium droplet when the oxygen supply was stopped and the temperature of the droplet decreased. Dendrite formation is expected to result in a highly porous sodium oxide structure.

SOFIRE II calculates the heat release from sodium reaction with oxygen assuming that the reactions involve an unvarying proportion of the formation of sodium oxide and sodium peroxide per unit mass of oxygen consumed. At 298.15 K, the heats of formation of sodium oxide and sodium peroxide [13] are

$$\Delta H_{Na_2O}=-418.0\,\text{kJ/mol}\quad,$$

$$\Delta H_{Na_2O_2}=-513.2\,\text{kJ/mol}\quad.$$

On a per unit mass of sodium basis, these are

$$\Delta H_{Na_2O}=-9091\,\text{kJ/kg of Na}=-3911\,\text{Btu/lb of Na}\quad,$$

$\Delta H_{Na_2O_2} = -11162\,\text{kJ/kg of Na} = -4801\,\text{Btu/lb of Na}$.

The values assumed in SOFIRE II are -3900 and -4500 Btu/lb of Na, respectively.

Sodium reacts as vapor with oxygen in a flame zone. To calculate the actual heat release for each reaction, it is necessary to add the enthalpy of vaporization of sodium. At 298.15 K, the sodium heat of vaporization [13] is

$\Delta H_{vap,Na} = 107.3\,\text{kJ/mol} = 4667\,\text{kJ/kg of Na}$.

The net heat release from the reaction of condensed phase sodium with oxygen is thus

$\Delta H_{Na_2O,net} = -4423\,\text{kJ/kg of Na}$,

$\Delta H_{Na_2O_2,net} = -6494\,\text{kJ/kg of Na}$.

Since the reaction rate is limited by the transport of oxygen to the flame zone, the net heat releases should be compared on a per unit mass of oxygen basis. The ratio of sodium mass-to-oxygen mass is 2.88 for Na_2O and 1.44 for Na_2O_2. The net heat releases are

$\Delta H_{Na_2O,net} = -12712\,\text{kJ/kg of O}$,

$\Delta H_{Na_2O_2,net} = -9332\,\text{kJ/kg of O}$.

On a per unit mass of oxygen basis, the heat release for the burning of sodium to produce of Na_2O is 1.36 times that for the burning of sodium to produce Na_2O_2.

As discussed above, sodium peroxide can be dissolved by sodium by the reaction,

$Na_2O_2 + 2Na \rightarrow 2Na_2O$.

When this happens, the reaction is exothermic releasing 322.8 kJ/mol of Na_2O_2 dissolved.

When sodium oxide is transformed to sodium peroxide in the presence of an abundance of oxygen according to,

$$Na_2O + \frac{1}{2}O_2 \rightarrow Na_2O_2 \quad ,$$

the reaction is exothermic releasing 95.23 kJ/Mol of Na_2O_2 formed.

Newman states that the mean measured burning rate for sodium pools of greater than 0.1 m diameter in ambient air is 10.5 kg/(m^2·s) [5]. At a temperature of 600 °C, the sodium density is 811 kg/m^3. For this value, the height of a sodium pool, neglecting the effects of oxides sinking into the pool, decreases at a rate of 1.29×10^{-5} m/s or 4.66 cm/hour (1.83 in/hour).

For a sodium pool fire inside of a closed volume, the above sodium burning rate should be typical of the initial value. The mass of oxygen inside of a closed volume will decrease with time such that the mass transport of oxygen to the pool upper surface decreases with time causing the sodium burning rate to decrease with time from the initial value.

2.2 Aerosol Formation and Behavior

Sodium pool burning is accompanied by the formation of a significant amount of aerosols/smoke. SOFIRE II ignores aerosol formation except for the definition of an effective emissivity for the gas above the pool reflecting the presence of aerosols in the gas.

Newman presented a curve for the fraction of sodium reacted that was measured as smoke [2]. The smoke fraction is equal to 0.11 for pool temperatures between 250 and about 600 °C above which it increases to about 0.26 at 670 °C and 0.38 at 760 °C. Newman suggests that the unvarying smoke fraction between 250 and 600 °C is related to the transport of sodium through the oxide wicks on the pool surface [2]. Above 600 °C, there exists a liquid metal sodium pool surface from which sodium vaporization occurs. The aerosol formation fraction increases with temperature above 600 °C because the sodium vapor pressure increases with temperature.

The sodium atmospheric boiling temperature is 881.55 °C. Sodium oxide (Na_2O) melts at 920 °C, begins to vaporize at 1350 °C, and boils above 1600 °C [1414]. The solid sublimates at 1275 °C at a low pressure of 0.06 bar. Sodium peroxide (Na_2O_2) is stated to decompose slowly at 280 °C, melt at 510 °C, and decompose into Na_2O and oxygen at 510 to 545 °C [14]. Sodium is more volatile than the oxidic reaction products such that aerosol formation is due to the reaction of sodium vapor with oxygen.

The aerosols formed have been found to be Na_2O_2 [15]. Sodium peroxide is highly hygroscopic and will react with available moisture in air to form sodium hydroxide [15],

$$Na_2O_2 + H_2O \rightarrow 2\,NaOH + \frac{1}{2}O_2 \quad ,$$

releasing 78.73 kJ/mol of Na_2O_2 reacted. The sodium hydroxide formed reacts with available carbon dioxide in air to form sodium carbonate and sodium hydrocarbonate according to the reactions [15],

$$2\,NaOH + CO_2 \rightarrow Na_2CO_3 + H_2O \quad ,$$

$$Na_2CO_3 + CO_2 + H_2O \rightarrow 2NaHCO_3 \quad .$$

Sodium hydroxide is white, melts at 318.4 °C, and boils at 1390 °C [16]. Sodium carbonate is white and melts at 851 °C [16].

In experiments at the Kernforschungszentrum Karlsruhe (KfK) involving dilute sodium fire aerosols in air with loadings between 0.5 and 1.25 g/m^3 and a mean aerodynamic diameter of 0.7 µm, almost all particles were transformed to carbonate after 18 and 27 seconds, at relative humidities of 40 and 70 %, respectively. For the carbonated aerosols produced from 40 % relative humidity, 15 % of the carbonate aerosols were transformed into hydrocarbonate.

However, earlier tests performed at Atomics International at a relative humidity below 30 % showed that the aerosols were mainly oxide and that conversion to sodium hydroxide was slow. Of course, in a closed volume, the masses of water vapor and carbon dioxide available to react with aerosols are limited.

In the sodium pool fire tests conducted in the FAUNA facility at KfK, the median particle diameters inside of the vessel varied with time from 0.5 to 0.8 µm initially, increasing rapidly to 2 to 3 µm, and decreasing to 0.5 µm several hours after the fire. The interpretation is that small particles of about 0.5 µm median diameter are formed from condensation following the reaction of sodium vapor with oxygen in the flame zone but larger particles are then produced due to coagulation while small particles are lost to diffusion and deposition upon surfaces. After the fire, the larger particles settle out leaving smaller particles.

It is of interest to investigate the nature of the aerosol cloud. For particles that absorb all of the incident electromagnetic radiation, the intensity of radiation decreases with distance through the cloud according to the Beer-Lambert law,

$$I(x) = I(0) \exp\left(-\pi r^2 n x\right) ,$$

where

I = intensity,

r = particle radius,

n = number of particles per unit volume,

x = distance.

The particle number density is given by

$$n = \frac{M_{aerosol}}{\rho_{aerosol} \frac{4}{3} \pi r^3 V_{compartment}} .$$

The intensity thus decreases by 95 % after penetration through a distance,

$$x_{pen} = \frac{3}{\pi r^2 n} = \frac{4 \rho V_{compartment} r}{M_{aerosol}} .$$

SOFIRE II does not model the effects of aerosols in the gas phase above the sodium pool. In particular, the heat capacity effects of aerosols in the gas phase are not modeled. Aerosol formed directly heat the atmosphere above the pool as it intermixes with the gas phase.

SOFIRE II does model thermal radiation heat transfer from the pool surface to the aerosol-bearing atmosphere above the pool using an effective emissivity between the pool surface and the aerosol. The effective emissivity would be expected to be given by

$$\varepsilon_{\text{eff}} = \frac{1}{\frac{1}{\varepsilon_{\text{pool surface}}} + \frac{1}{\varepsilon_{\text{atmosphere}}} - 1}.$$

Yamaguchi and Tajima report that Hashiguchi et. al. measured an emissivity of 0.65 for the oxidized surface of a burning sodium pool [17]. For an atmosphere containing a dense aerosol (i.e., one through which thermal radiation does not penetrate in a straight shot manner as discussed above) consisting of Na_2O_2, this same emissivity might be assumed for the atmosphere. Emissivities need to be identified for use in describing aerosols consisting of sodium hydroxide and sodium carbonate particles.

3 Previous Extensions of SOFIRE II

There have been some noteworthy extensions to the modeling in SOFIRE II. A code named SOFIRE-MII was developed at what is now the Japan Atomic Energy Agency (JAEA) [18]. It is stated that its numerical procedures and treatments of heat transports have been improved extensively in SOFIRE-MII. A code named ASSCOPS was developed as a pool-spray mixed combustion code; its pool combustion model was taken from SOFIRE-MII. JAEA also developed a code called SPM that added modeling for sodium vaporization off of the liquid metal sodium pool surface and reaction with oxygen inside of a flame zone distinct from the pool surface. The paper doesn't reference review papers such as those of Newman stressing how the burning rate is limited by the transport of oxygen. In comparing with data they calculated that oxygen transport is what limits the burning and in the conclusions to their paper stated that although SPM has an advantage over SOFIRE-MII and ASSCOPS in modeling the combustion process, it could not be clearly demonstrated; the conventional model in SOFIRE-MII/ASSCOPS predicts the overall combustion process just as well.

Marimuthu at the Indira Gandhi Centre for Atomic Research in India developed a revision of the SOFIRE II one-cell model that he named SFIRE1C [19]. He sought to remove two major deficiencies of SOFIRE II. The first is the assumption that the relative proportions of Na_2O and Na_2O_2 formed from the interaction of oxygen and sodium are assumed in SOFIRE II to remain unvarying throughout the calculation. He incorporated modeling whereby combustion is divided into two phases; only Na_2O is formed during the first phase followed by the formation of only Na_2O_2 during the second phase. He assumed that the transition between the first and second phases occurs after a user input time. He assumed times of 30 and 45minutes in comparisons with experiments. He did not incorporate a transition from Na_2O_2 back to Na_2O should the pool temperature rise above 600 °C, although his paper notes the existence of this phenomenon.

The second deficiency that Marimuthu sought to remove was the lack of modeling for aerosol formation. He calculated rates of aerosol formation based upon rates of sodium vaporization from a liquid metal pool. He assumed the correlation of Schütz and Sauter who measured vaporization rates of sodium from a contaminated sodium pool into an overlying argon or nitrogen cover gas for pool temperatures between 437 and 723 °C [20]. They presented a temperature dependent correlation for the vaporization rate which Marimuthu incorporated into his code. They also noted that the vaporization rates that they measured were approximately proportional to the sodium vapor pressure. Matrimuthu noted that in using the correlation the effects of an oxide layer on the pool surface or the presence of flames near to the surface are neglected. In comparing with data, he concluded that a reasonable estimate of the aerosol concentration was achieved.

4 First Principles Investigation of a Sodium Pool Fire

Consider the postulated release of the inventory of an intermediate circuit loop from the sodium storage vessel of that loop for a 100 MWe Sodium-Cooled Fast Reactor (SFR) incorporating a supercritical carbon dioxide Brayton cycle power converter. It is assumed that there are two intermediate loops each having a sodium inventory of 11,100 kg. The sodium storage vessel for each loop is assumed to be installed inside of its own airtight compartment having a length of 8.5 m, width of 6 m, and height of 7 m. Release of 11,100 kg of sodium onto the 51 m^2 floor creates a sodium pool having an initial depth of 0.268 m. Assuming an initial compartment temperature of 60 °C, the initial air density is 1.067 kg/m^3 such that the total air mass in the 357 m^3 volume neglecting the volume of the sodium storage vessel is 381 kg. The oxygen is initially 23.2 % of the air by weight providing an initial oxygen mass of 82.8 kg. If this mass is completely consumed in the formation of Na_2O through burning of sodium, then the sodium mass consumed is 238 kg. Thus, the fire will go out due to lack of oxygen with no more than 238 kg of the sodium burned. In fact, the flammability limit for sodium burning by oxygen in air is 3 % oxygen such that the fire may go out before 238 kg of sodium is reacted. Over the floor area, this sodium mass represents only 0.575 cm of the sodium pool depth. At an initial burning rate of 4.66 cm/s, it would require only 7.4 minutes to burn the sodium. Assuming that the burning rate is proportional to the oxygen weight fraction in the air in the compartment, the burning rate will decrease exponentially with time with a time constant equal to that calculated assuming the initial burning rate. For an exponential decay, three times the burning time at the initial burning rate is the time to consume 95 % of the oxygen. Thus, the required time is 22.2 minutes. This example illustrates the effectiveness of compartmentalization in limiting the amount of oxygen available such that a sodium pool fire will quickly burn itself out when the oxygen is consumed.

Assuming that 11 % of the burned sodium equal to 26.2 kg gives rise to the formation of aerosols, the Na_2O_2 aerosol mass formed is 44.4 kg. It is assumed that the compartment initial temperature in 60 °C. If the atmosphere is saturated with water vapor at this temperature, then the water vapor density is 0.130 kg/m^3 and the water vapor mass at 100 % relative humidity is 46.5 kg. To convert all of the Na_2O_2 aerosol to NaOH requires 10.3 kg of water vapor. This can be accomplished for relative humidities greater than 22.1 %. Thus, if the relative humidity were 50 %, there would be more than enough water vapor to convert the sodium peroxide aerosol to sodium hydroxide aerosol. The CO_2 mass needed to further convert the aerosol to sodium carbonate is 25.1 kg. However, the carbon dioxide weight fraction in air is only 0.00046 such that there is only 0.175 kg of CO_2 in the compartment atmosphere. Thus, very little carbonate can form. Conversion to sodium hydroxide increases the aerosol mass by only 2.59 % to 45.6 kg. Sodium hydroxide melts at 318.4 °C such that the “aerosol” could consist of liquid drops depending upon the temperature.

For a sodium peroxide aerosol, the sodium peroxide theoretical density is 2805 kg/m^3. Assuming a median particle diameter of 3.0 µm such that the median particle radius is 1.5 µm and that the particles are fully dense, a penetration depth for electromagnetic radiation of 0.14

m is calculated. Thus, the aerosol will be a smoke cloud through which there is no straight shot path for radiation.

5 SOFIRE-II Code Implementation at ANL

The SOFIRE II code was obtained from the Radiation Safety Information Computational Center (RSICC) located at Oak Ridge National Laboratory. As delivered, the code actually consists of the two versions discussed in the user report [1], SOFIRE II ONE CELL and SOFIRE II TWO CELL. The former has been implemented at ANL. The SOFIRE-II ONE CELL code version was compiled with Intel Fortran on a PC. Some modifications needed to be implemented in the code to allow use of the text files for input/output (I/O) processing. In the original version, the I/O operations were done using a terminal keyboard and monitor. Simple modifications to the code were introduced to read the input data from the "Input.txt" file and write the results to the "Output.txt" file. In addition, the same results are now written to an "Output_Tab.txt" file in a table form to facilitate plotting with Microsoft EXCEL or other similar software.

In addition, two typographical errors in the codes equations were found and corrected. In the previous version, the thermal resistance of the second concrete node was incorrectly used in the equations for the third and fourth nodes. These were replaced with the correct resistances for these nodes which were calculated in the code but weren't used. This correction did not change the results much since the concrete temperature is usually a slowly changing variable and the thermal resistances of the concrete nodes are similar, unless significantly different node thicknesses are selected.

5.1 Verification of Test Problem Results

To verify that the newly compiled version of the SOFIRE-II code ONE CELL version produces the correct results, the calculation of the test problem was run The input and output of the test problem were provided with the code; the results of the test problem were also plotted in the code report [1].

The results of the test problem are presented in Figure 1 which shows the time dependency of calculated variables versus the original results from the code report (shown in red as the upper of each pair of plots in Figure 1). The newly obtained results (lower plots) provide values that are close to those reported in the code report. In general, each pair of the plots in Figure 1 has the same scale on both axes; the only exception is the *Cell Floor Concrete Temperature* plot, which is discussed below.

The results in Figure 1 show very good agreement between the newly obtained results and those reported previously, although some differences were observed. After some analysis, it was concluded that the differences are attributed to the accuracy of the calculations. The most significant differences are observed for the *Cell Floor Concrete Temperature* plots. In this case, the calculated derivatives are small due to large masses and were close to the original code accuracy. With the single-precision accuracy used by default in Fortran for real numbers, the cell floor temperature of 598.4 °R, for example, is stored in the code as

598.4000. If the calculated temperature change per time step is less than 10^{-4} (or, more accurately, less than $0.5*10^{-4}$ to account for rounding up), no temperature change will be calculated within this code accuracy. This was the case between about 2 and 4 hours for the cell floor temperature plots in Figure 1 where the temperature is reported to be constant. Even if the temperature is calculated to change, it follows from the above discussion that the temperature change per time step can only be a multiple of 10^{-4} resulting in the piecewise linear behavior of this temperature plot. Since the results obtained with the modern compiler are somewhat smoother, it seems that the accuracy in the original calculation was even less than 10^{-4} for this temperature. Note that this difference was observed for the cell floor temperature only which was the slowest changing temperature in the calculation. All other results show very close agreement between the two calculations, although they are not exactly identical.

The fact that the observed differences are due to the code accuracy was indirectly confirmed by switching to double precision calculations for all real numbers. As demonstrated in Figure 2, the double-precision calculation produced much smoother temperature curves for the concrete walls than that with single precision. Since the smooth temperature behavior is more physical in the absence of other external events (which was the case in this calculation), it is demonstrated then that the results with single precision and those obtained with the original code were indeed lacking accuracy for the concrete wall temperature. It is therefore recommended to keep the double precision accuracy option enabled for the further calculations with the SOFIRE-II code as is the case for the calculations discussed below.

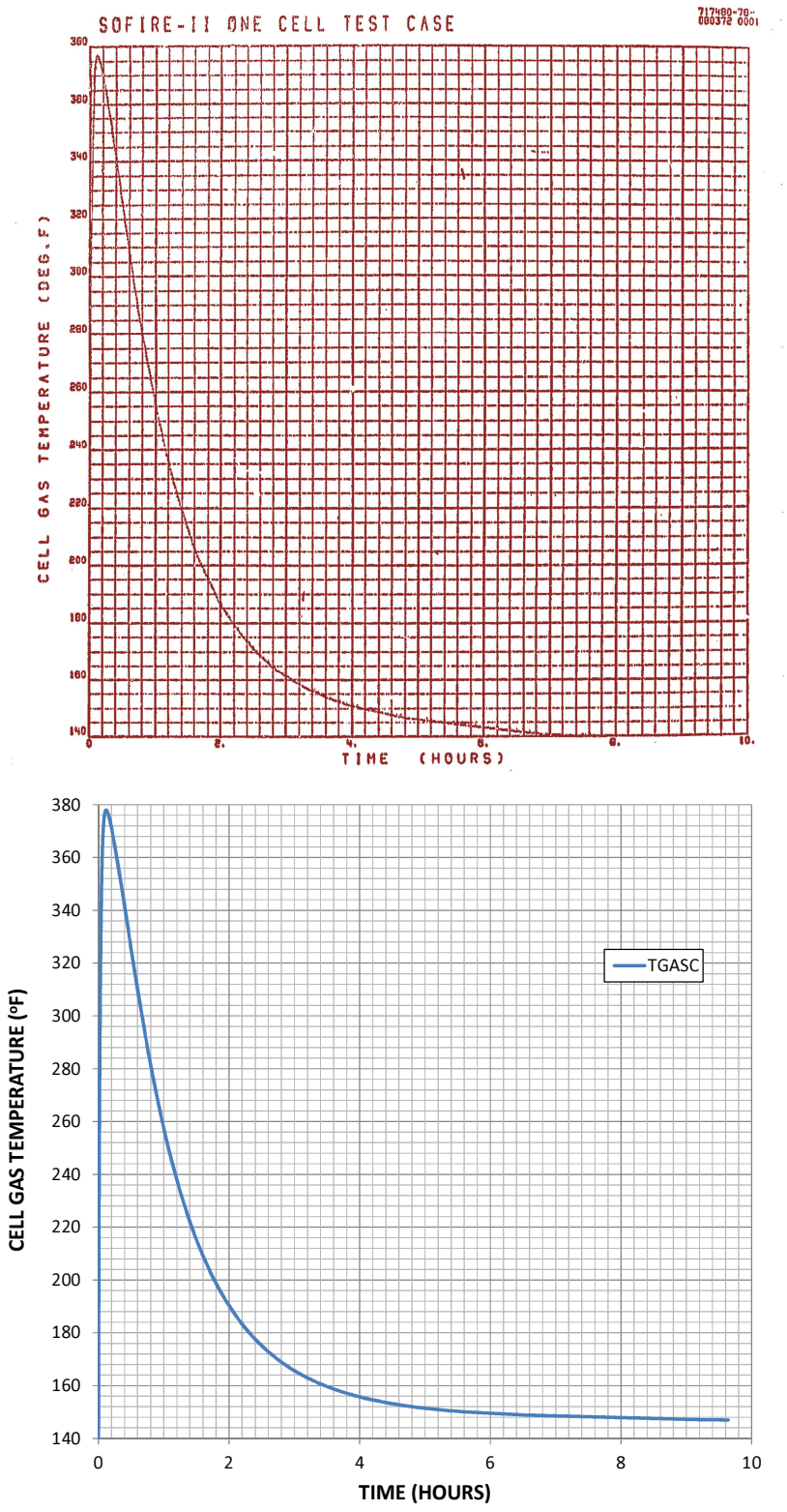

Figure 1. Verification of the Test Case Results.

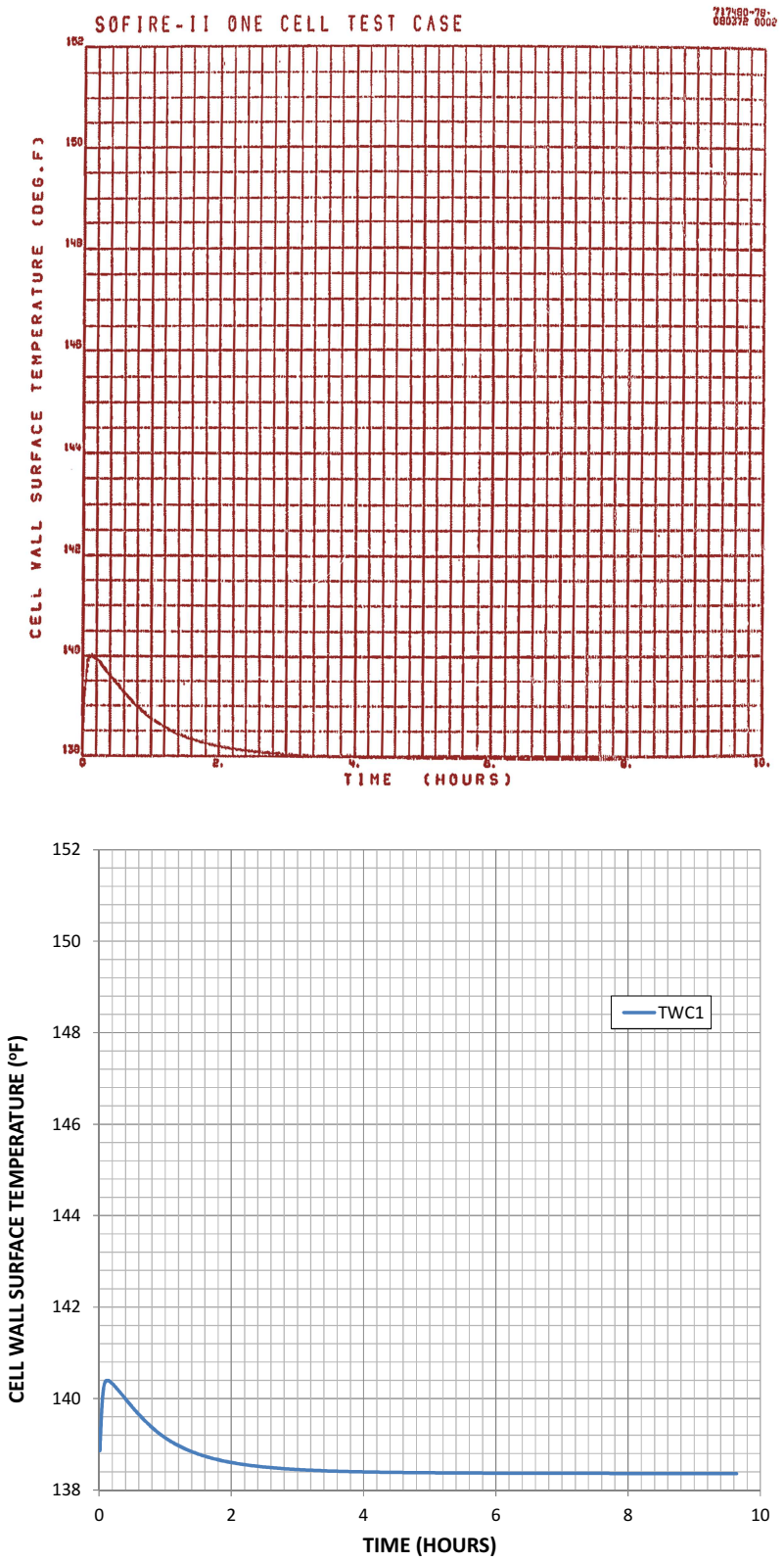

Figure 1. Verification of the Test Case Results. (Continued).

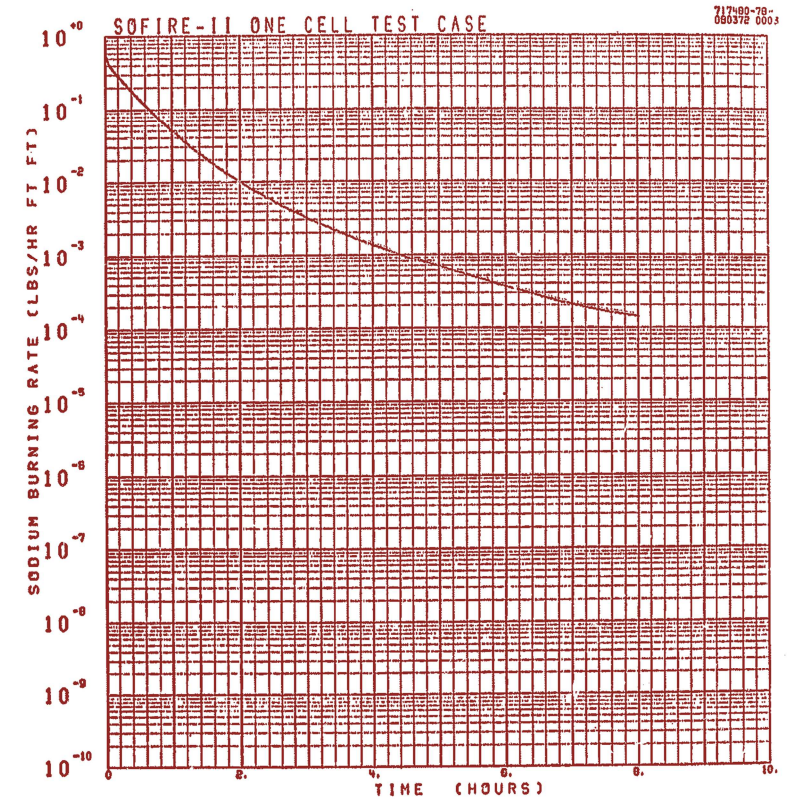

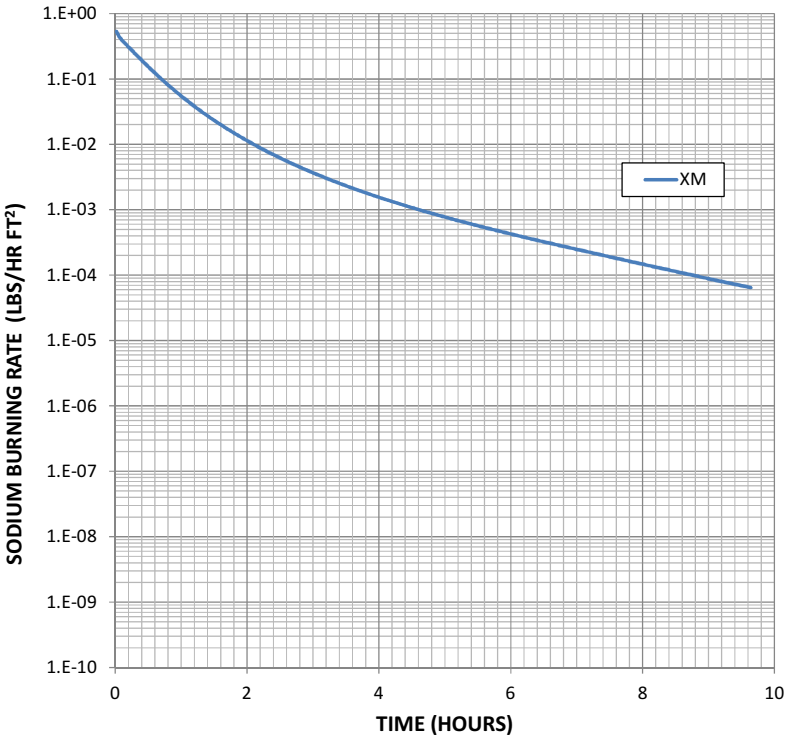

Figure 1. Verification of the Test Case Results. (Continued).

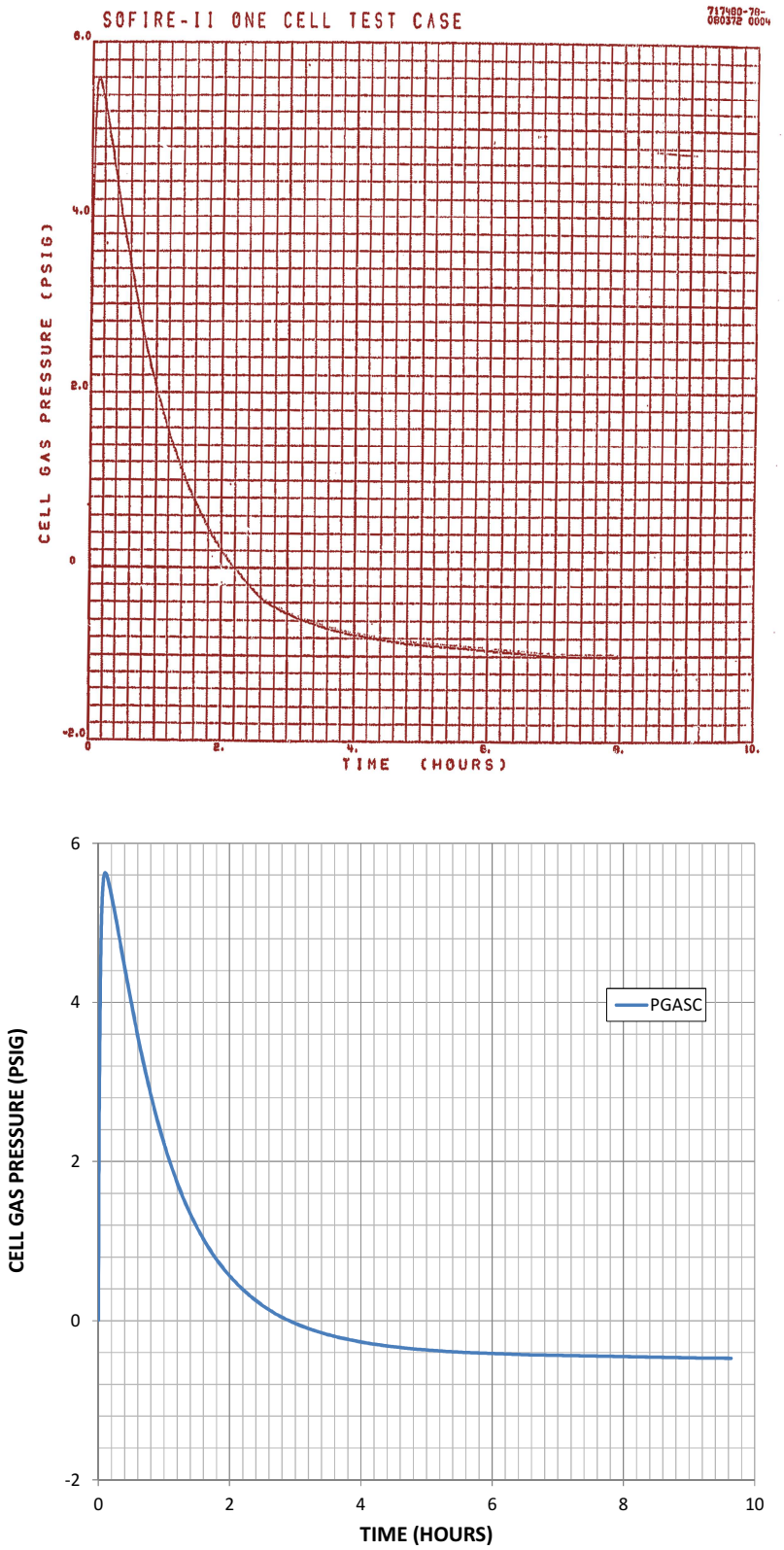

Figure 1. Verification of the Test Case Results. (Continued).

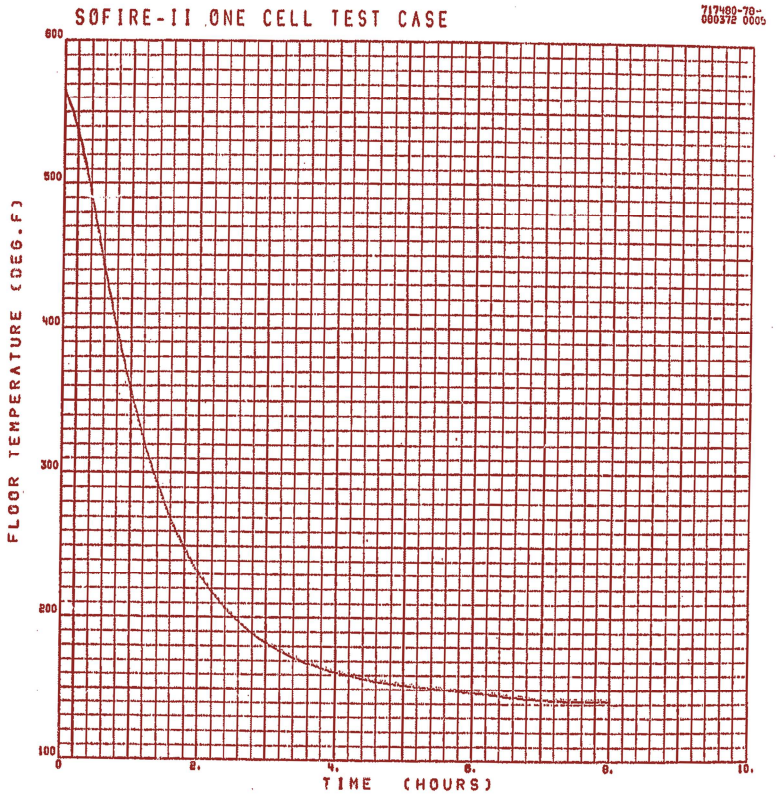
SOFIRE-II ONE CELL TEST CASE
FLOOR TEMPERATURE (DEG.F)
600
500
400
300
200
100
0
2.
4.
6.
8.
10.
TIME (HOURS)

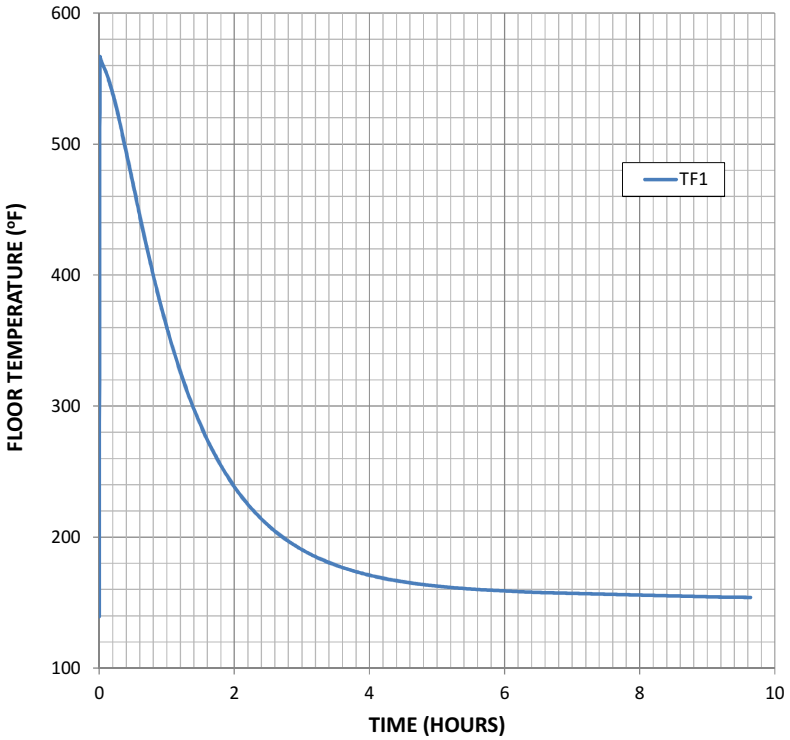

Figure 1. Verification of the Test Case Results. (Continued).

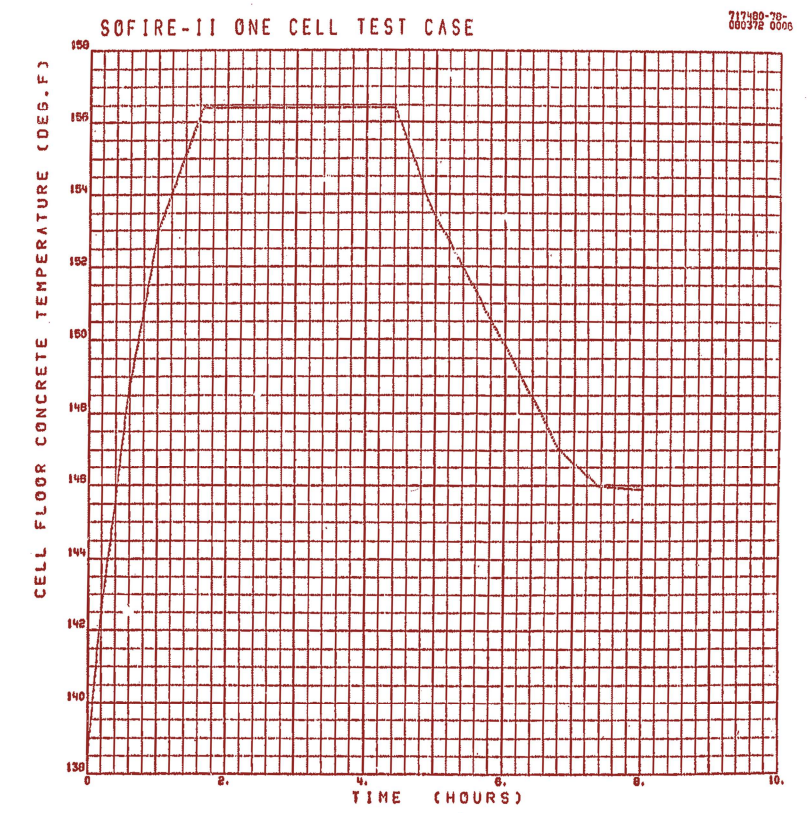

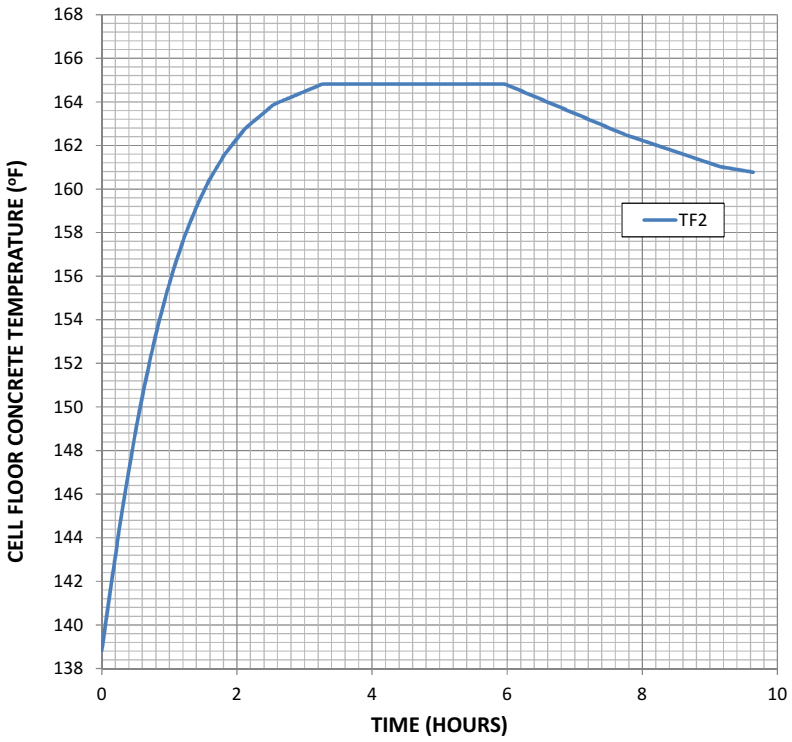

Figure 1. Verification of the Test Case Results. (Continued).

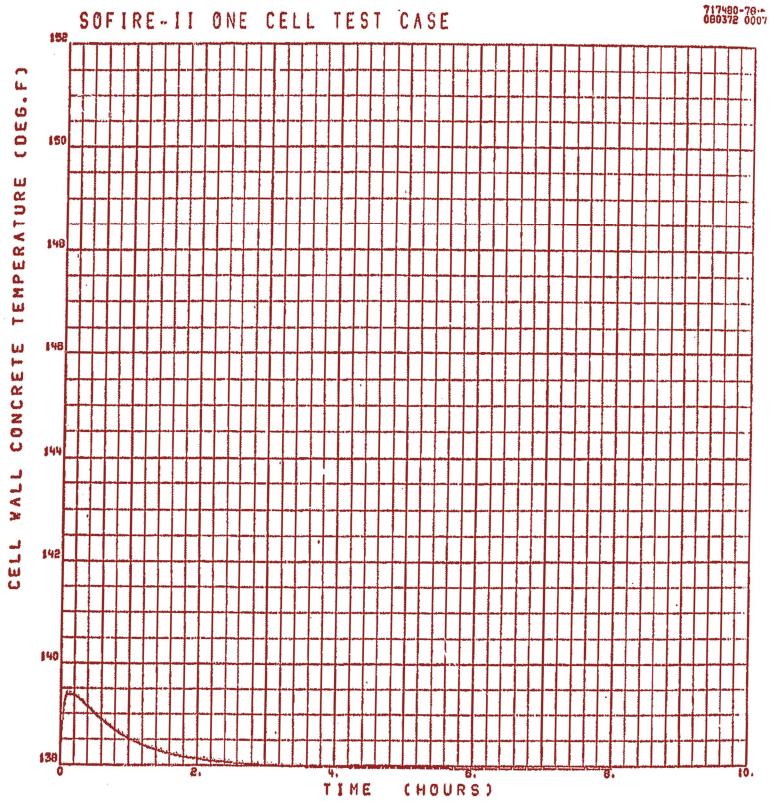
SOFIRE-II ONE CELL TEST CASE
CELL WALL CONCRETE TEMPERATURE (DEG.F)
TIME (HOURS)

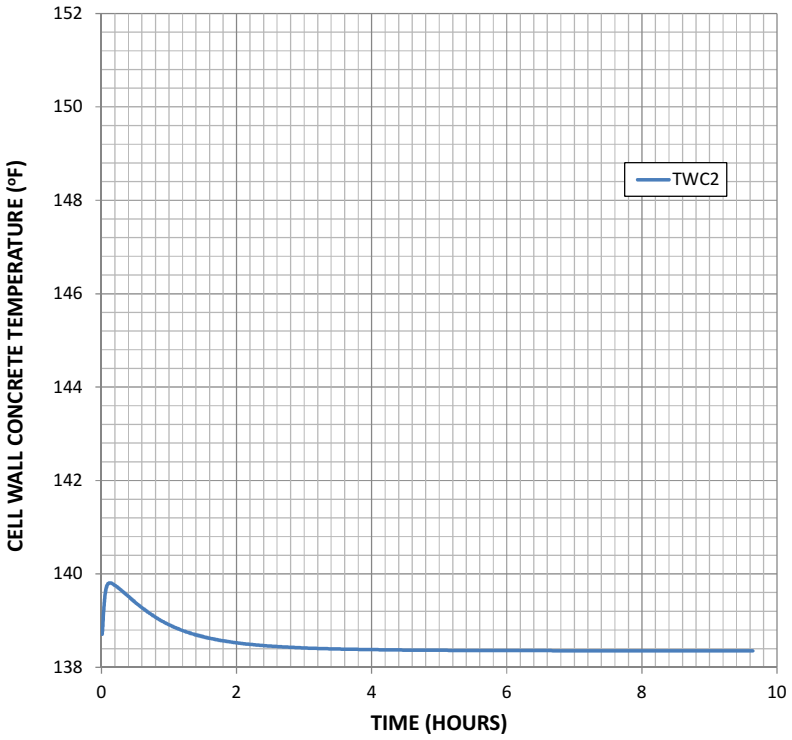
CELL WALL CONCRETE TEMPERATURE (°F)
TIME (HOURS)
TWC2

Figure 1. Verification of the Test Case Results. (Continued).

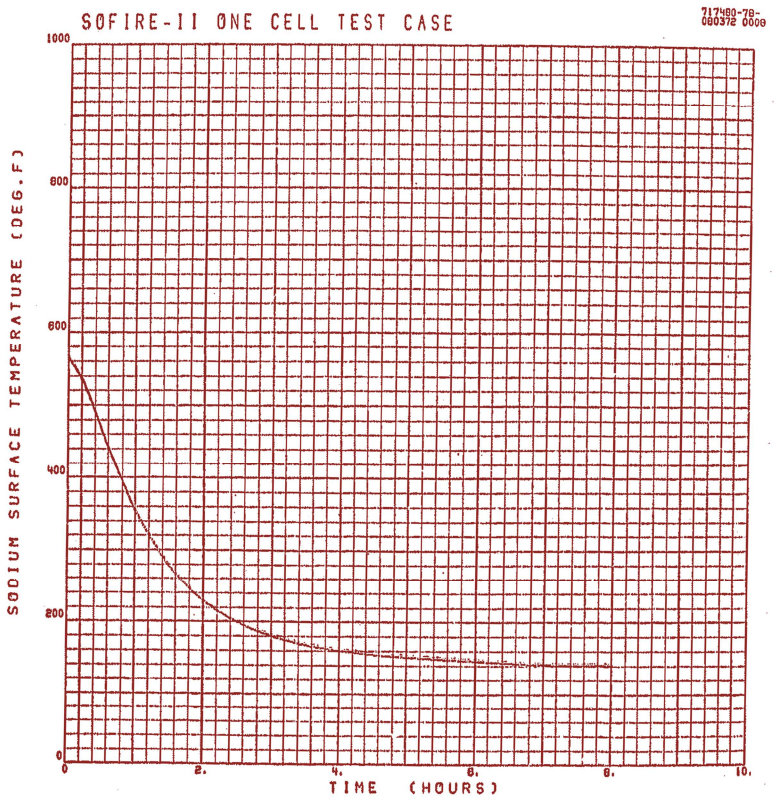

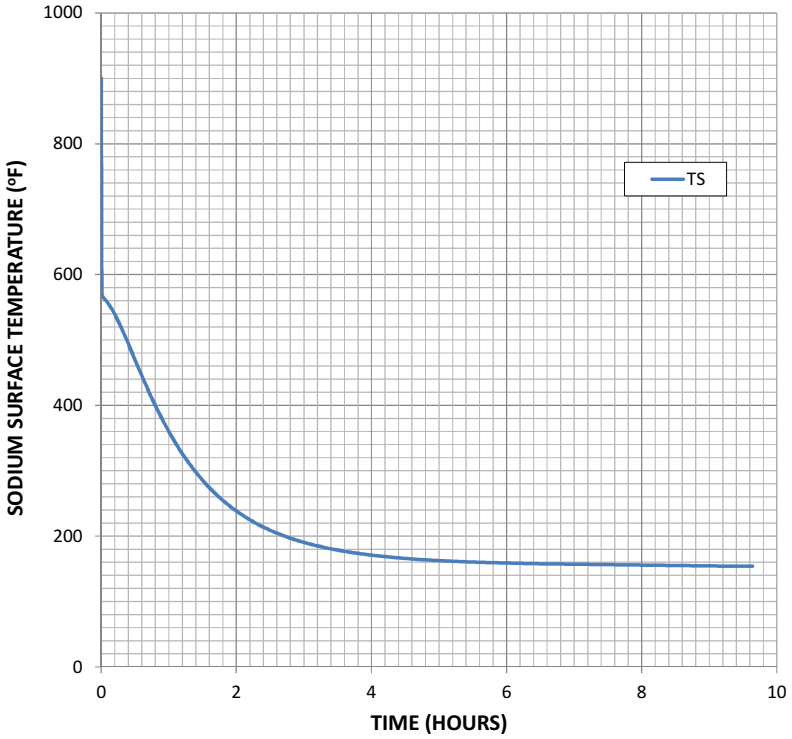

Figure 1. Verification of the Test Case Results. (Continued).

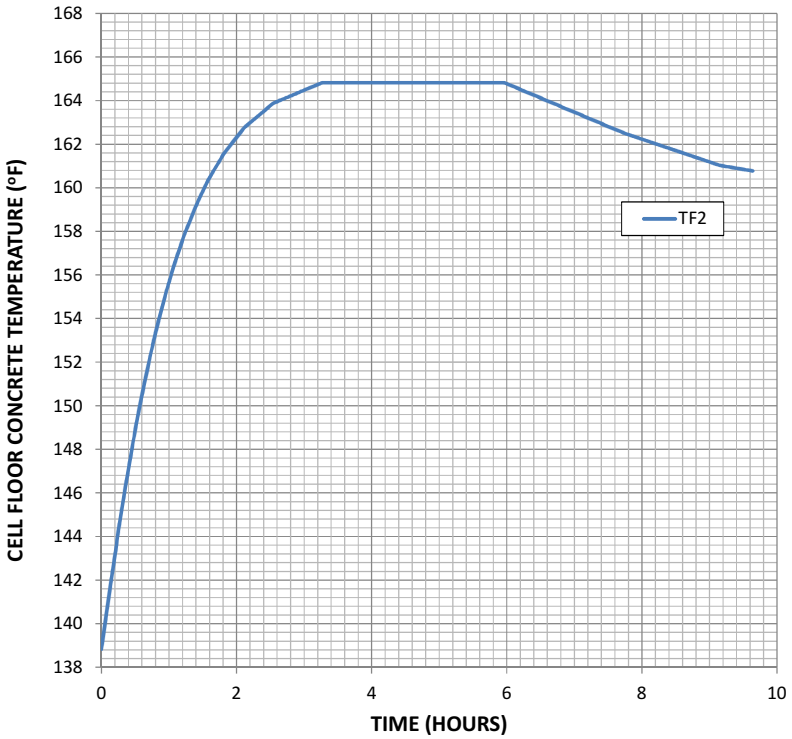

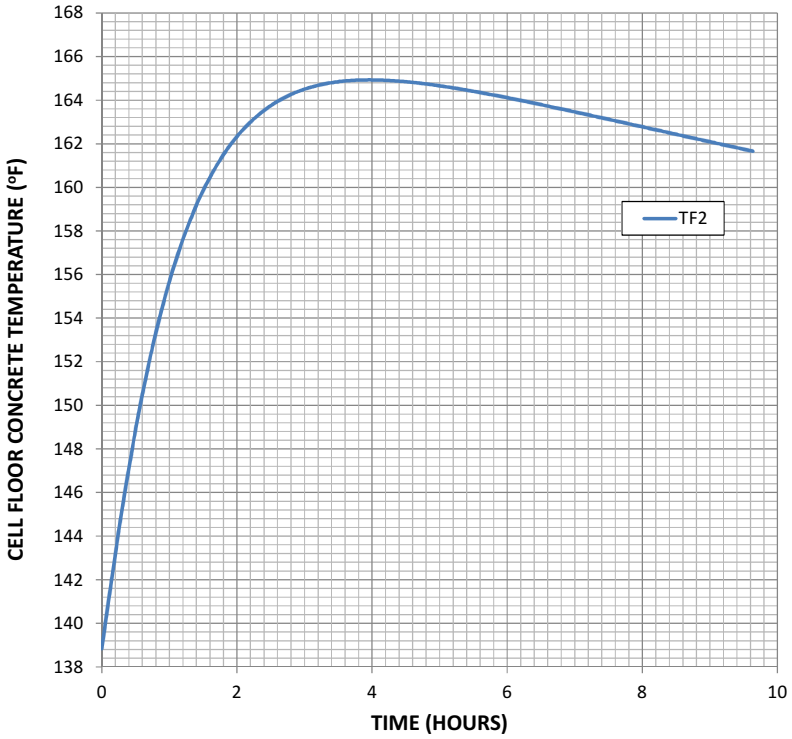

Figure 2. Cell Floor Temperature with Single (Top) and Double (Bottom) Precision Calculations.

6 SOFIRE II Preliminary Calculations for the AFR-100

Unlike the above first principles example, the AFR-100 incorporates a superheated steam cycle. There are four intermediate heat transport circuit loops in two pairs; each pair serves a single twisted tube intermediate heat exchanger (IHX) located inside of the reactor vessel. Each of the four intermediate sodium loops has a single 70 MWt steam generator. There are two steam generator options. The first is a straight tube steam generator (STSG) and the second is a helical coil steam generator (HCSG). The helical coil steam generator design significantly reduces the number of tubes relative to the straight tube steam generator design but the intermediate sodium volume inside of the helical coil steam generator is greater than that for the straight tube steam generator. Table 1 shows the component and total sodium volumes for each of the four intermediate circuit loops for the two steam generator options. The intermediate sodium volume in the IHX, 0.463 m^3, is actually the sodium from both loops serving the IHX. It is conservatively assumed that all of the IHX intermediate sodium could potentially drain in the event of a rupture of one of the loops.

The internal volume of the sodium storage vessel (i.e., dump tank) for each loop is assumed to be 20 % greater than the sodium volume of an intermediate loop. The storage vessel is assumed to consist of a cylindrical central section onto which hemispherical heads are welded. The length of the central cylindrical section is assumed to be equal to the cylindrical section/hemispherical head diameter. Thus, the storage vessel length is twice the diameter and the storage vessel internal volume, V, is related to the diameter, d, by

$$V = \frac{5}{12}\pi d^3 .$$

This equation is solved for the storage vessel internal diameter. The vessel internal length is twice the diameter.

To determine the storage vessel outer dimensions, the storage vessel stainless steel wall is assumed to 2.54 cm (1.0 in) thick and surrounded by 0.3048 m (1.0 foot) of thermal insulation.

To determine a minimum size for the compartment in which the storage vessel is installed, it is assumed that a minimum of 2.0 meters for personnel access is provided between the outside of the thermally insulated storage vessel and the walls. This provides the compartment widths and heights shown in Table 1. The compartment height is taken equal to the width.

Table 1. Sodium Volumes for One Intermediate Sodium Loop, Sodium Storage Vessel Dimensions, and Storage Vessel Compartment Dimensions.

Steam generator (SG) option	Straight tube	Helical coil
SG intermediate sodium volume, m^3	19.19	29.37
Intermediate sodium piping volume, m^3	2.07	0.91
IHX intermediate sodium volume (two loops) , m^3	0.46	0.46
Total intermediate sodium volume per loop, m^3	21.72	30.74
Intermediate sodium storage vessel internal volume, m^3	26.07	36.89
Intermediate sodium storage vessel inner diameter/length, m	2.710/5.421	3.043/6.086
Intermediate sodium storage vessel outer diameter/length including thermal insulation , m	3.37/6.08	3.70/6.75
Intermediate sodium storage vessel compartment dimensions, width/length /height, m	7.4/10.1/7.4	7.7/10.8/7.7

The SOFIRE II ONE CELL code was applied to calculate a sodium pool fire resulting from a postulated rupture of the sodium storage vessel of one of the AFR-100 intermediate sodium loop resulting in drainage of all of the intermediate sodium from that loop onto the floor of the storage vessel compartment. For the two steam generator options, the widths and heights of the storage vessel compartments are not that different. Therefore, calculations are performed only for the larger compartment for the helical coil steam generator option. The compartment width and height are thus taken equal to 7.7 m. The compartment length in Table 1 is 10.8 m. However, in the calculations, a somewhat greater length of 11.4 m is assumed; that is an additional 0.3 m of space is available between each end of the storage vessel and the neighboring wall.

The volume taken up by the storage vessel inside of the compartment is not subtracted from the compartment volume. This is a conservative assumption in terms of the amount of sodium that can be burned, although the heat up of the compartment gas atmosphere and potentially the gas pressure rise might be underestimated. For example, if air can ingress into the intermediate sodium loop, then air can be drawn into the intermediate loop as the sodium drains onto the compartment floor. The volume internal to the floor, walls, and ceiling of the compartment is 676 m^3 which is much greater than the internal volume of the sodium storage vessel and the intermediate loop sodium volume.

The intermediate sodium high and low temperatures are assumed to equal 528 and 373 °C, respectively. SOFIRE II requires an initial temperature for the sodium which is thus taken equal to the mean of the high and low temperatures or 450 °C. At this temperature, the sodium density is 846 kg/m^3 such that the sodium mass drained onto the floor is 26,010 kg. SOFIRE II assumes that the sodium mass/volume collects upon the floor instantaneously. Over the 87.8 m^2 floor area, the initial sodium pool depth is 0.350 m.

SOFIRE II divides the sodium pool into five axial layers of which the surface layer reacts with oxygen from the overlying gas atmosphere and transfers heat by natural convection and thermal radiation to the overlying gas atmosphere. In the present calculation, the layer thicknesses are defined to be identical. Thermal conduction is calculated between the five layers. Convection within the sodium pool is neglected. This may be expected to be a reasonable approximation given the high sodium thermal conductivity and the fact that a configuration in which the sodium temperature is highest at the upper surface and lowest at the lower surface should be a thermally stable configuration. The sodium-to-oxygen burning ratio is set to 2.88 for the formation of sodium oxide, Na_2O, as the reaction product. The input variable for thermal radiation from the pool upper surface to the overlying gas atmosphere is set equal to unity and the variable for thermal radiation from the pool upper surface to the walls is set equal to zero because the atmosphere above the pool is expected to become filled with a cloud of aerosols.

SOFIRE II models a steel liner on the floor and walls of the compartment. The liner thickness is assumed equal to 6.35 mm (0.25 in); the liner is described with the thermophysical and transport properties for steel provided in the code test case problem. A gap is assumed between the floor liner and the underlying concrete floor. A gap thickness of 0.254 mm (10 mils) is assumed representative of a very narrow gap. SOFIRE II calculates thermal conduction across the gas in the gap; a thermal conductivity for air is input. The input variable for additional thermal radiation across the gap is set equal to unity. The meaning of the thermal radiation input variable is not discussed in the code user report [1]. If the variable for thermal radiation across the gap is meant to account for the emissivities of the liner and concrete surfaces facing each other, then the calculations below which set the variable equal to unity overestimates the effects of thermal radiation from the steel liner to the concrete.

SOFIRE II models three axial thermal conduction heat transfer cells below the liner and gap. The axial thicknesses of the three cells are carefully chosen to capture the essence of thermal conduction heat transfer into the underlying concrete over the timescale of the calculation. As will be seen below, the calculations are run over a time of three hours. A transient thermal wave penetrates approximately according to the formula,

$$\delta = \sqrt{12\,\alpha\,t} \quad ,$$

where

δ = thermal wave penetration depth,

α = concrete wall thermal diffusivity,

t = time.

Assuming the concrete thermophysical and transport properties provided in the code test case problem, the thermal diffusivity of concrete is calculated as 1.80×10^{-7} m^2/s for which the thermal wave penetration depth after three hours is 0.153 m. It is assumed that the concrete walls are at least this thick. The thickness of the first concrete cell is taken equal to the thickness of the steel liner. The lower surface of the third concrete cell is assumed to be at a depth of 0.153 m below the liner. The lower surface of the second concrete cell is assumed equal to the square root of the product of the depths of the lower surfaces of the first and third concrete cells below the air gap. This approach is appropriate for capturing thermal conduction effects with a few cells over a given timescale. The limitation of four cells for the floor liner and floor concrete in SOFIRE II reflects the limitations on computing power when the code was developed. Today, a large number of cells would be utilized to perform a more accurate calculation of thermal conduction into the liner, air gap, and concrete floor. The same assumptions and cell thicknesses are assumed for the liner and concrete walls of the walls which includes modeling of the compartment ceiling as part of the walls. Today, the ceiling would be modeled independently from the vertical walls and other structures inside the compartment, if they exist, would also be modeled for their heat sink effects.

Figure 3 through Figure 21 show the results calculated with SOFIRE II ONE CELL. Figure 3 shows that the oxygen mass inside of the compartment closed volume is consumed with the oxygen mass remaining reduced to 5 % of its initial value over 0.95 hour following the start of the calculation. The oxygen concentration in the air inside of the compartment falls from the initial value of 23.2 wt % to 3.0 wt % over a shorter time of 0.7 hour. The flammability limit is 3 vol % or higher such that the sodium pool fire would have been extinguished due to lack of sufficient oxygen after about 0.7 hour. SOFIRE II does not recognize flammability limits such that the code continues to calculate sodium burning/reaction as the mass of oxygen remaining tends to zero.

Figure 5 and Figure 6 present the sodium burning/reaction rate and the cumulative sodium mass burned versus time. Although 525 kg of sodium is calculated to be burned, a smaller mass of less than 490 kg would actually burn if the fire is extinguished after 0.7 hour when the oxygen concentration has fallen below the flammability limit.

The small mass of sodium burned relative to the total mass of sodium released onto the floor demonstrates the effectiveness of compartmentalization in limiting the effects of sodium fires by limiting the mass of oxygen available to react with the sodium.

Temperatures calculated at the upper surface of the sodium pool and inside the height of the sodium pool are shown in Figure 7 and Figure 8. The sodium temperature is greatest at the upper surface and decreases with depth through the sodium pool. After about 1 hour, the sodium temperatures are calculated to have virtually equilibrated across the pool height. The sodium temperatures initially rise with time due to the exothermic heat release due to reaction with oxygen but subsequently decrease due to heat losses to the heat sinks in the compartment.

The steel floor liner is calculated to be heated to nearly the temperature at the bottom of the sodium pool and virtually equilibrates with the sodium temperature after about one hour. Temperatures inside of the floor concrete beneath the gap below the steel liner are shown in Figure 10. Significant heatup of the concrete floor is calculated illustrating the effectiveness of the floor as a heat sink for removing thermal energy from the sodium pool. Temperatures inside of the steel wall liner and wall concrete are presented in Figure 11 and Figure 12 from which it is observed that the wall is also an effective heat sink.

Figure 13 through Figure 16 show conditions inside of the gas atmosphere. The gas is heated by thermal radiation and natural convection heat transfer from the upper surface of the sodium pool to the gas and cooled by natural convection heat transfer to the wall. The gas pressure inside of the closed compartment volume increases due to the heatup of the gas atmosphere. The pressure rise is less than that corresponding to the gas temperature rise due to reaction of oxygen with sodium which removes oxygen molecules from the gas atmosphere. After attaining a peak, the gas temperature and pressure decrease mainly due to heat losses to heat sinks together with continuing consumption of oxygen.

The calculated peak pressure of 0.163 MPa absolute implies that the compartment reinforced concrete walls, floor, and ceiling must be designed to withstand at least this internal pressure. Thus, the compartment must be hermetically sealed with a pressure retention capability.

Figure 17 through Figure 20 present various heat transfer rates during the sodium pool fire. Heat is lost from the pool upper surface mainly by thermal radiation.

SOFIRE II calculates a mass of aerosol released to the compartment atmosphere as shown in Figure 21. A mass of 142 kg of oxide is calculated to be released versus a mass of 525 kg of sodium burned. Assuming that the oxide is Na_2O, then the ratio of the sodium-to-sodium oxide mass is 0.742 such that the mass of sodium converted to aerosol is 105 kg. This is exactly 20 % of the 525 kg burned. Thus, it is deduced that SOFIRE II assumes that 20 % of the sodium mass burned forms aerosols. This is a greater fraction than the 11 % identified by Newman for sodium temperatures below 600 °C based upon experiments [2].

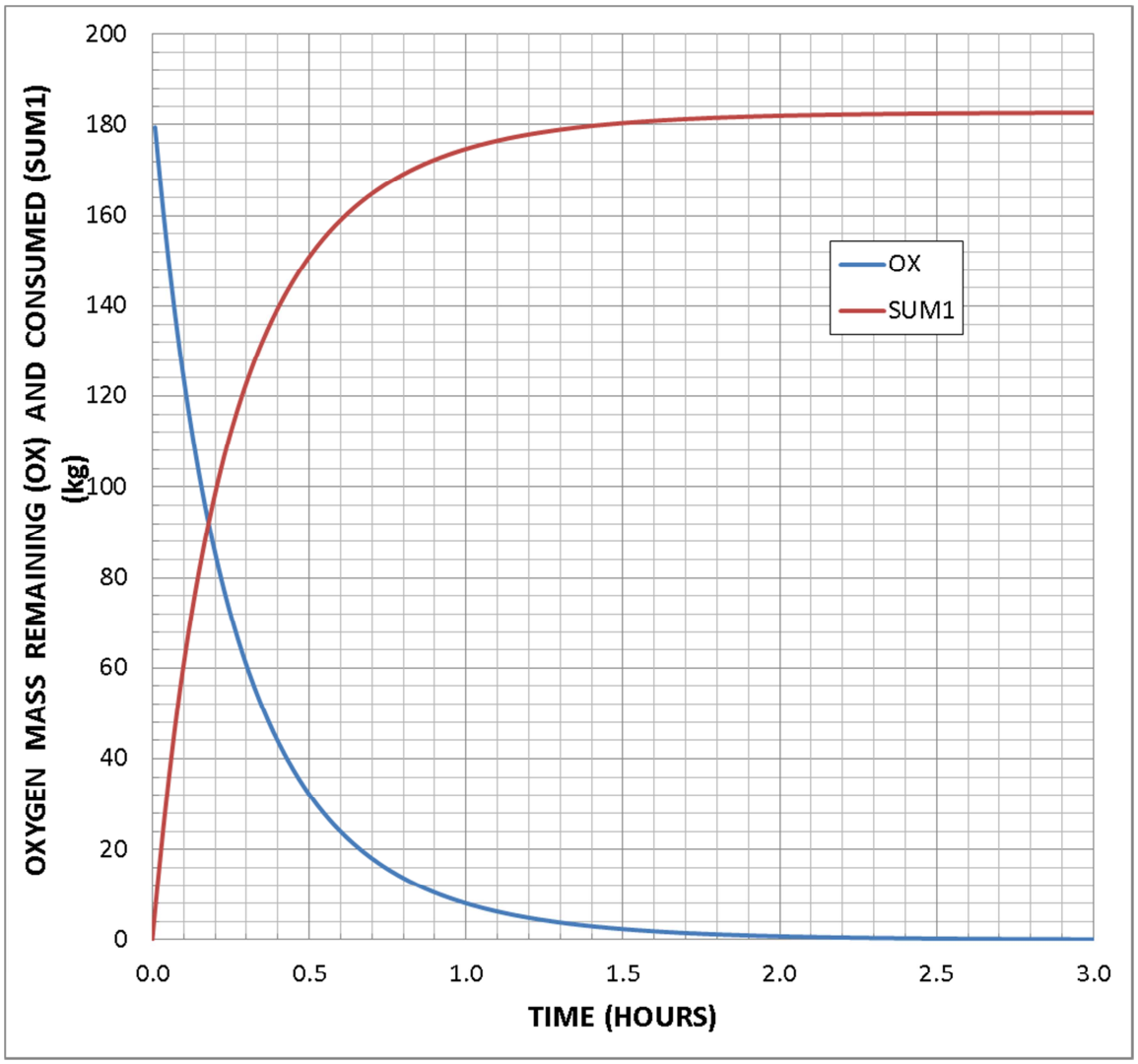

Figure 3. Oxygen Mass Remaining in Compartment Atmosphere versus Time for Sodium Pool Fire in Intermediate Sodium Storage Vessel Compartment.

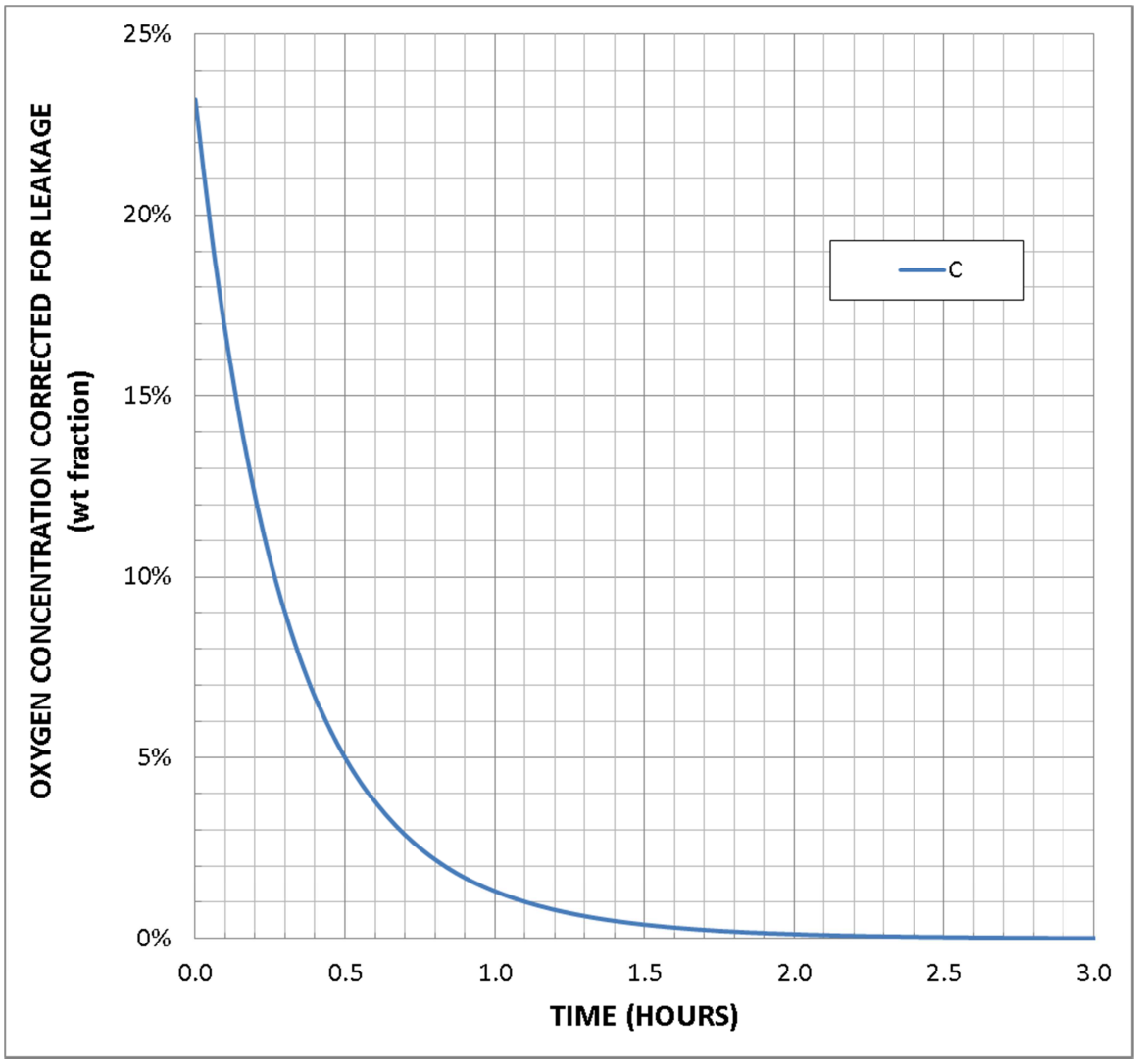

Figure 4. Oxygen Concentration in Compartment Atmosphere versus Time for Sodium Pool Fire in Intermediate Sodium Storage Vessel Compartment.

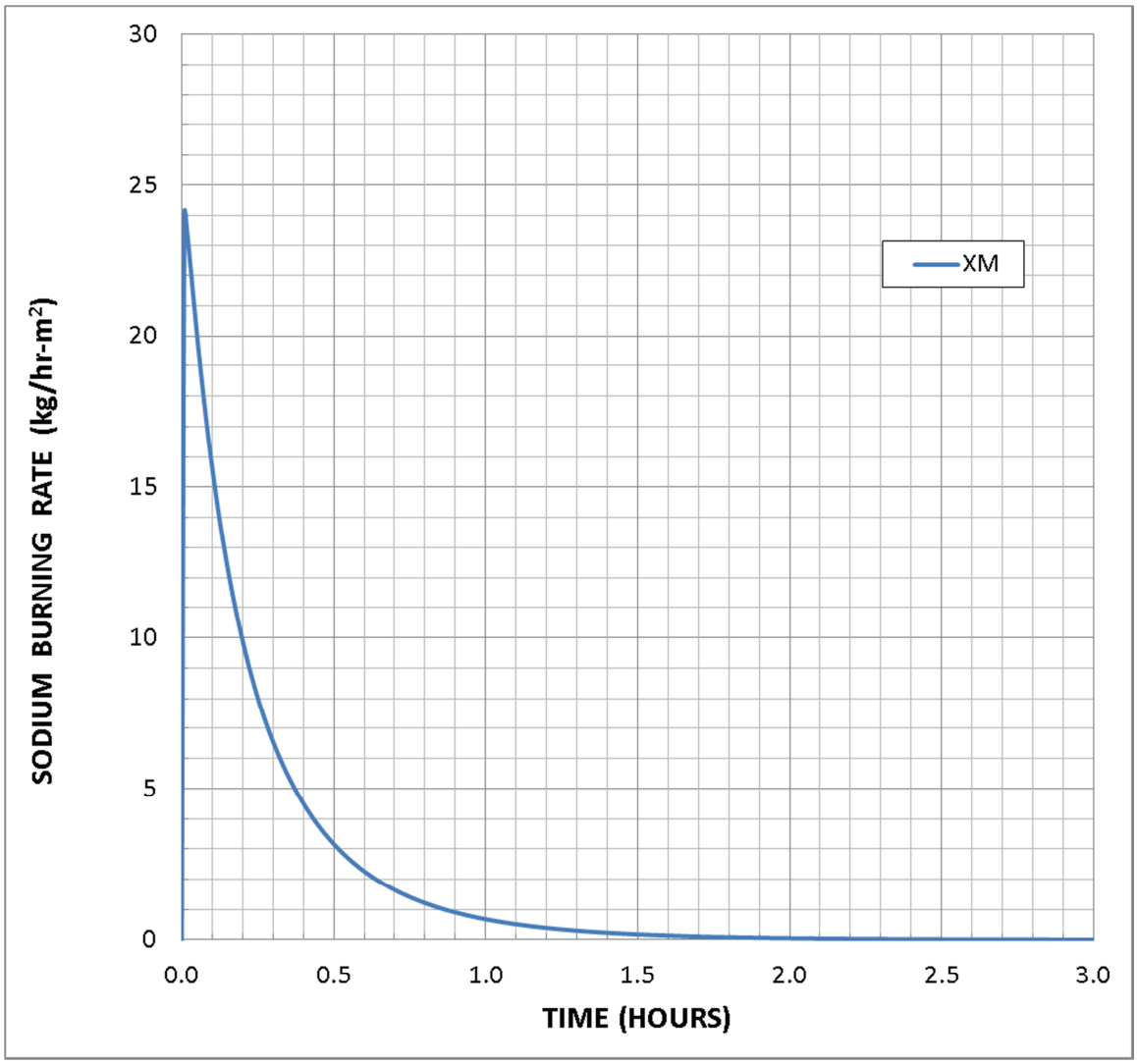

Figure 5. Sodium Burning Rate versus Time for Sodium Pool Fire in Intermediate Sodium Storage Vessel Compartment.

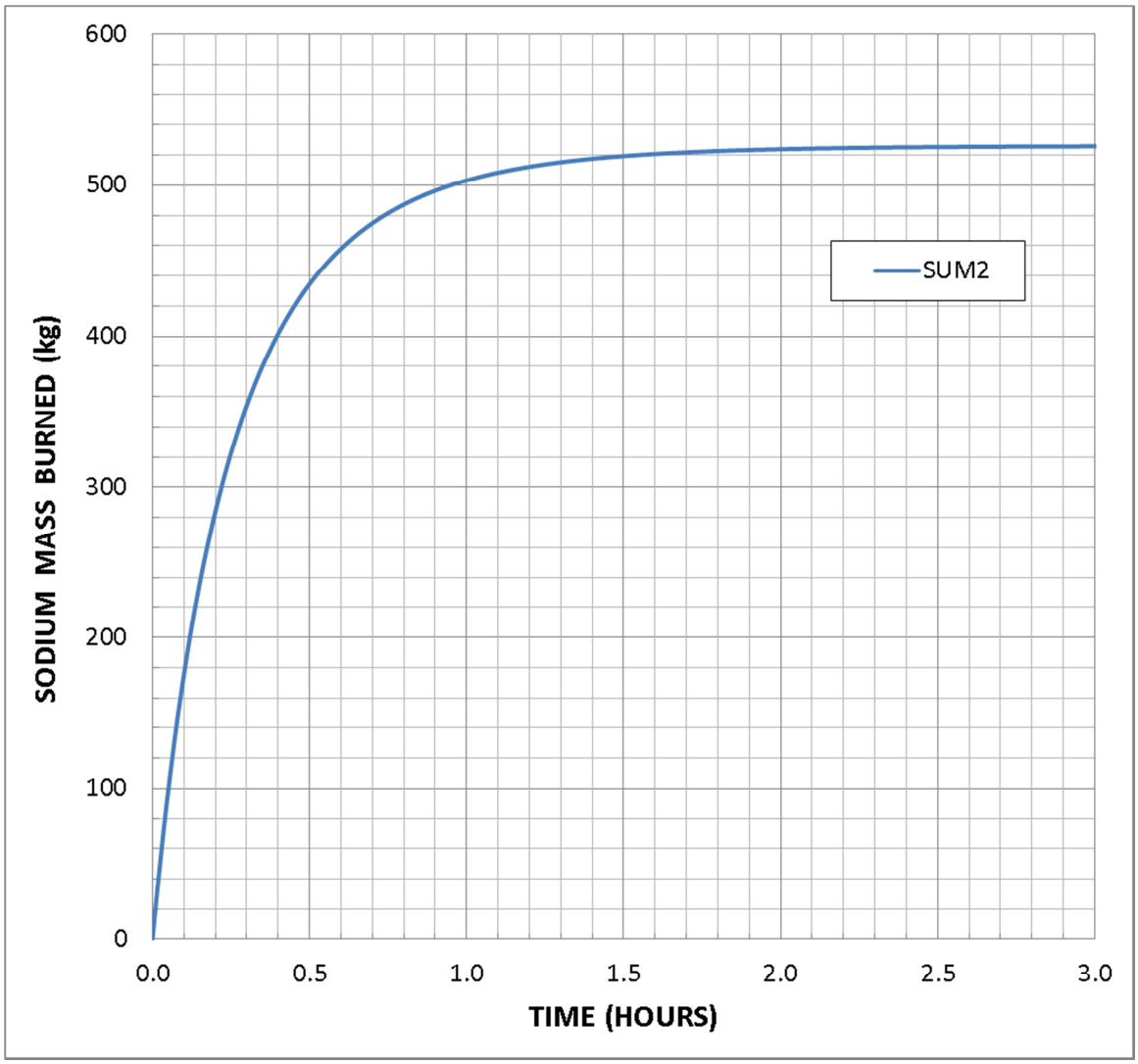

Figure 6. Cumulative Sodium Mass Burned versus Time for Sodium Pool Fire in Intermediate Sodium Storage Vessel Compartment.

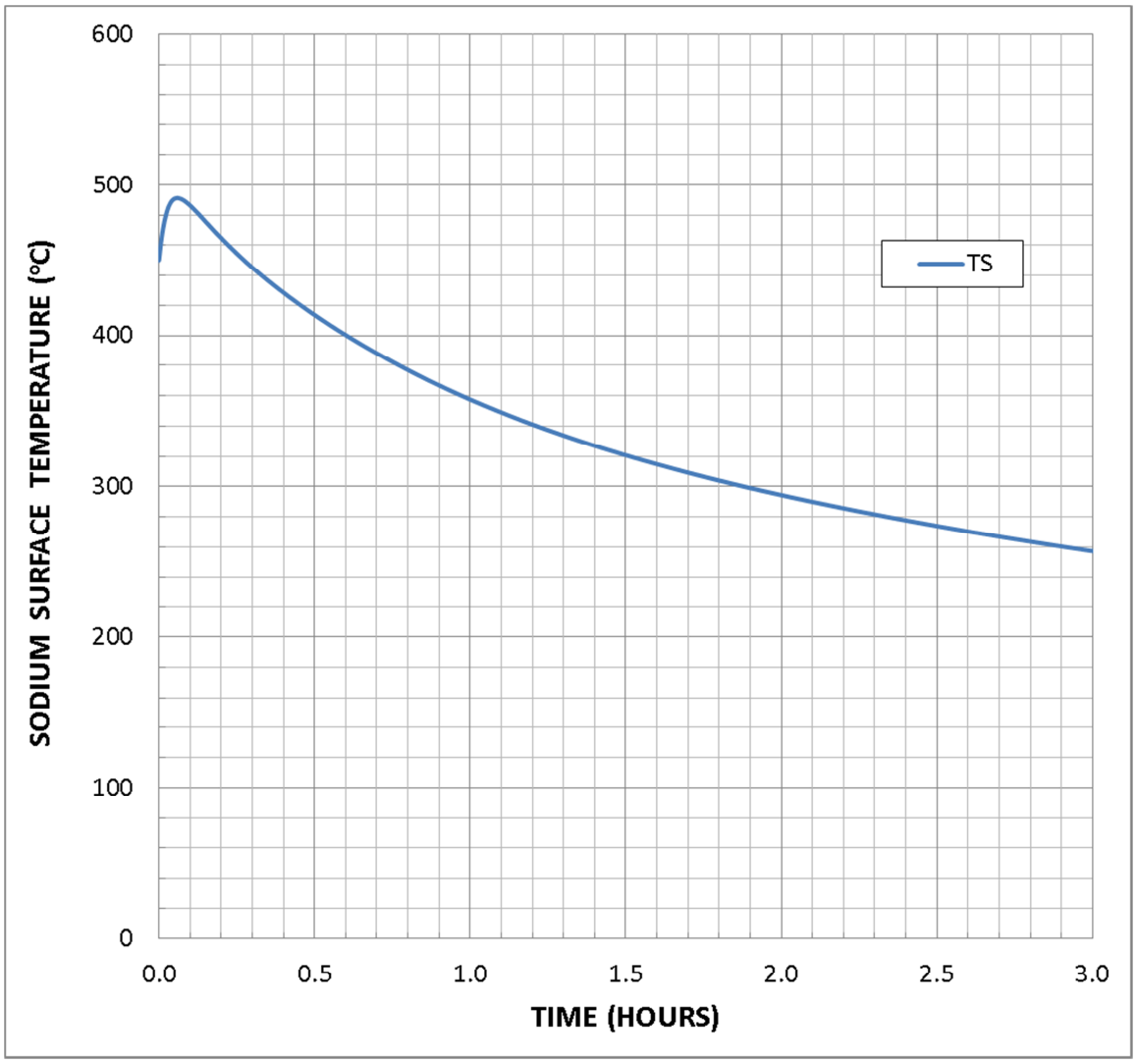

Figure 7. Sodium Upper Surface Node Temperature versus Time for Sodium Pool Fire in Intermediate Sodium Storage Vessel Compartment.

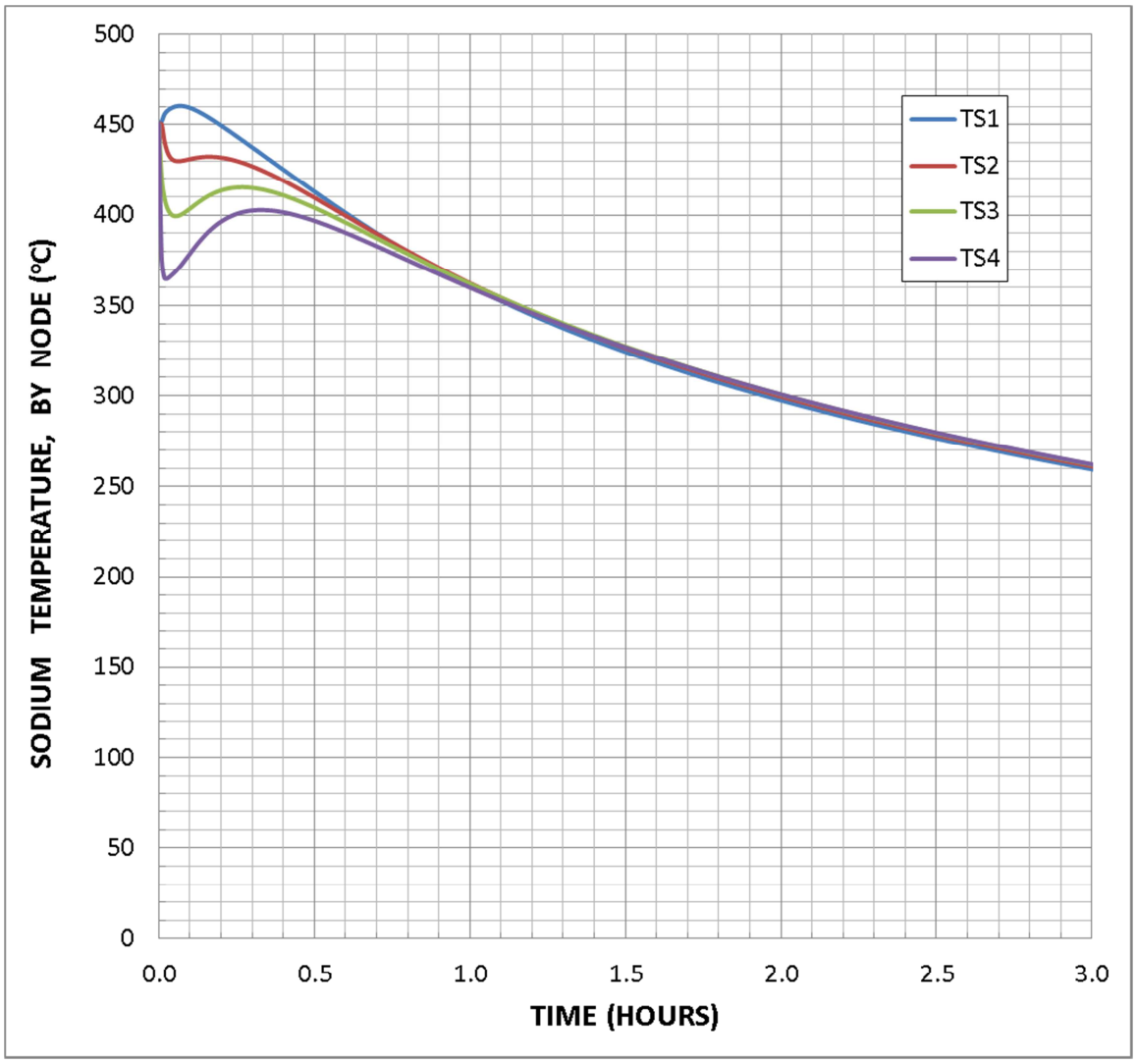

Figure 8. Temperatures of the Four Subsurface Nodes Inside of the Sodium Pool versus Time for Sodium Pool Fire in Intermediate Sodium Storage Vessel Compartment. The Sodium Pool Thickness is Divided into Five Equal Thickness Nodes Consisting of the Surface Node and Four Subsurface Nodes Beneath the Sodium Pool Upper Surface.

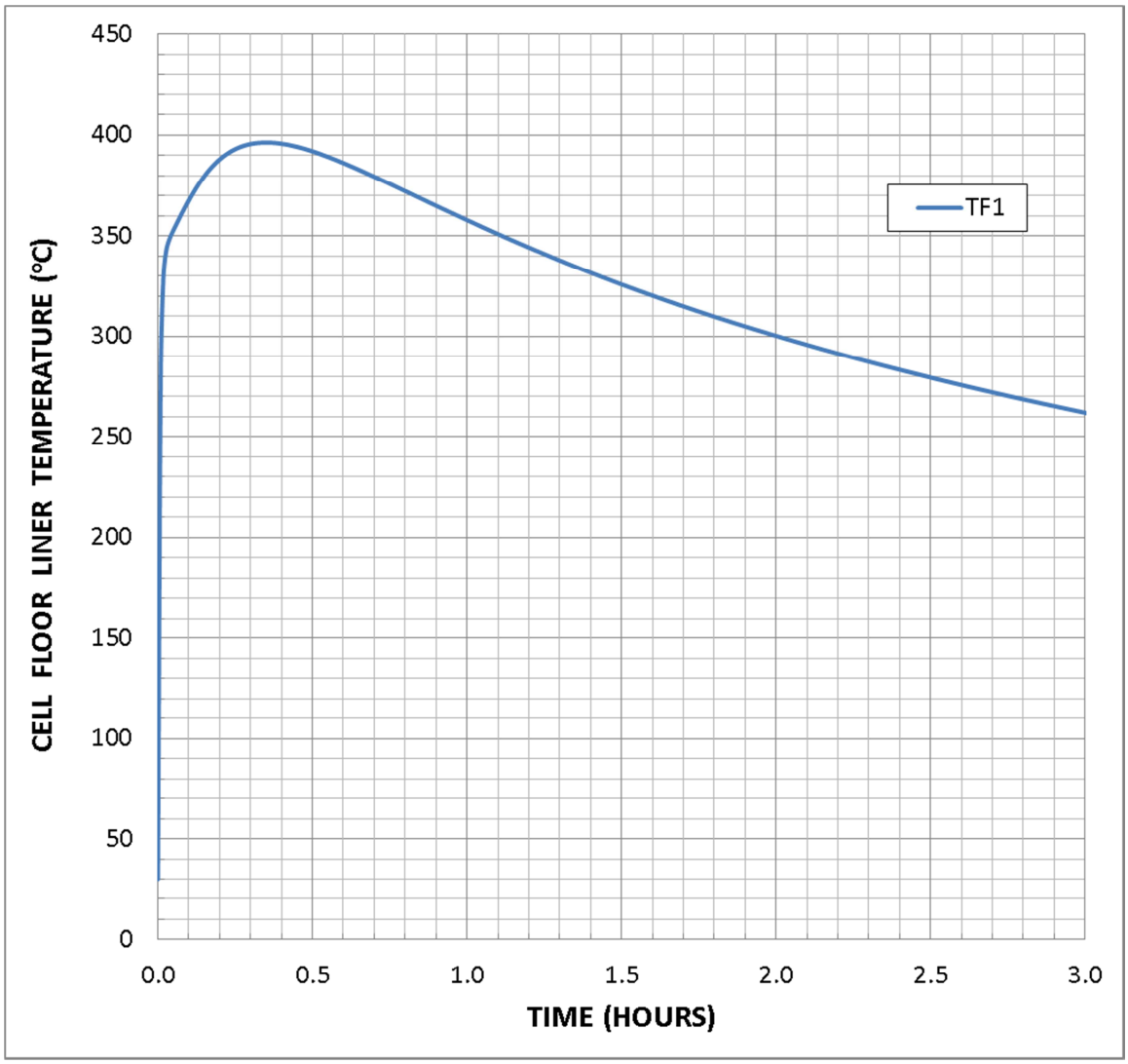

Figure 9. Temperature of Steel Floor Liner versus Time for Sodium Pool Fire in Intermediate Sodium Storage Vessel Compartment.

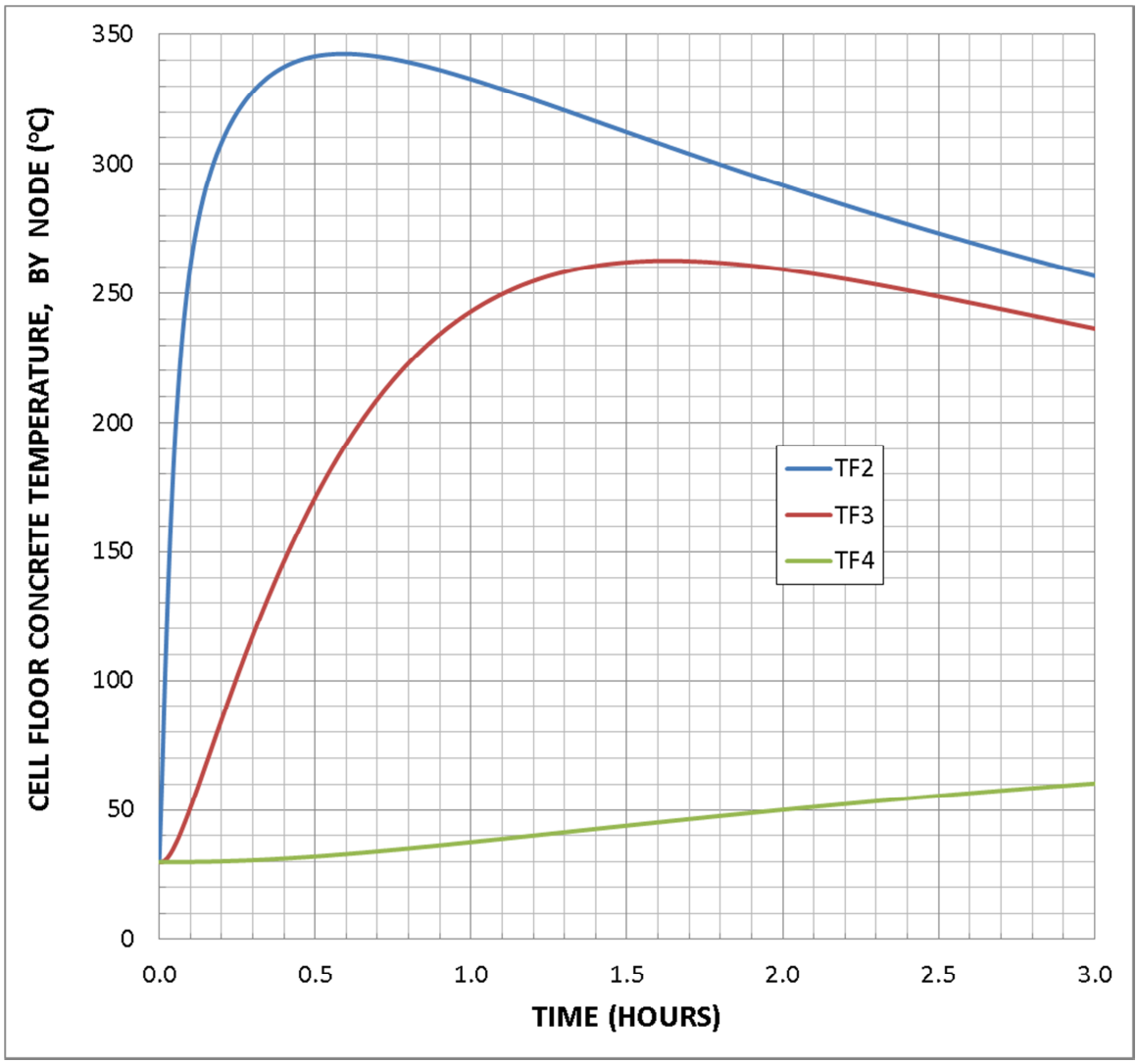

Figure 10. Temperatures Inside of Concrete Floor versus Time for Sodium Pool Fire in Intermediate Sodium Storage Vessel Compartment. The Concrete Floor Thickness Behind the Liner is Divided into Three Nodes of Increasing Thickness.

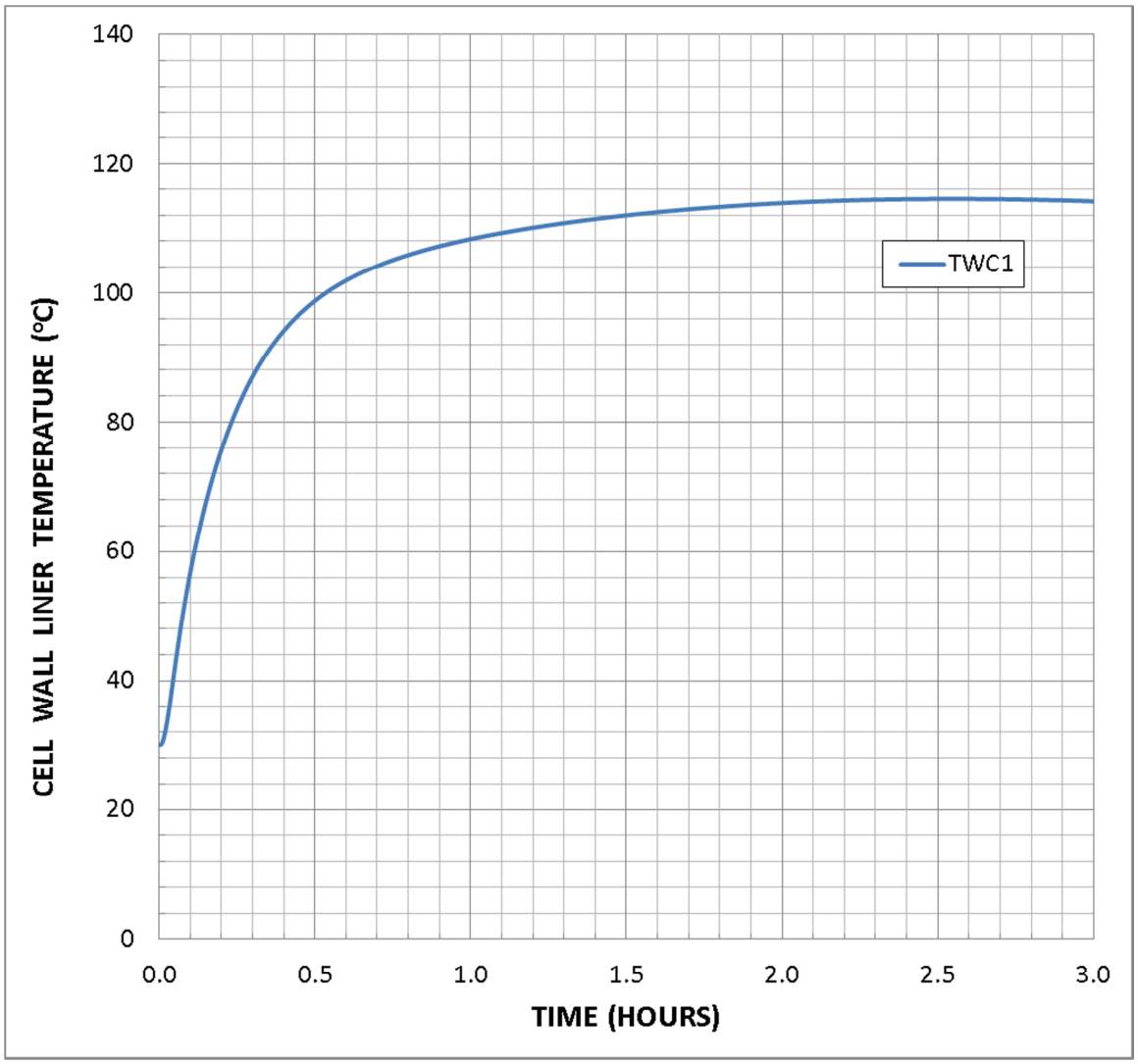

Figure 11. Temperature of Steel Wall Liner versus Time for Sodium Pool Fire in Intermediate Sodium Storage Vessel Compartment.

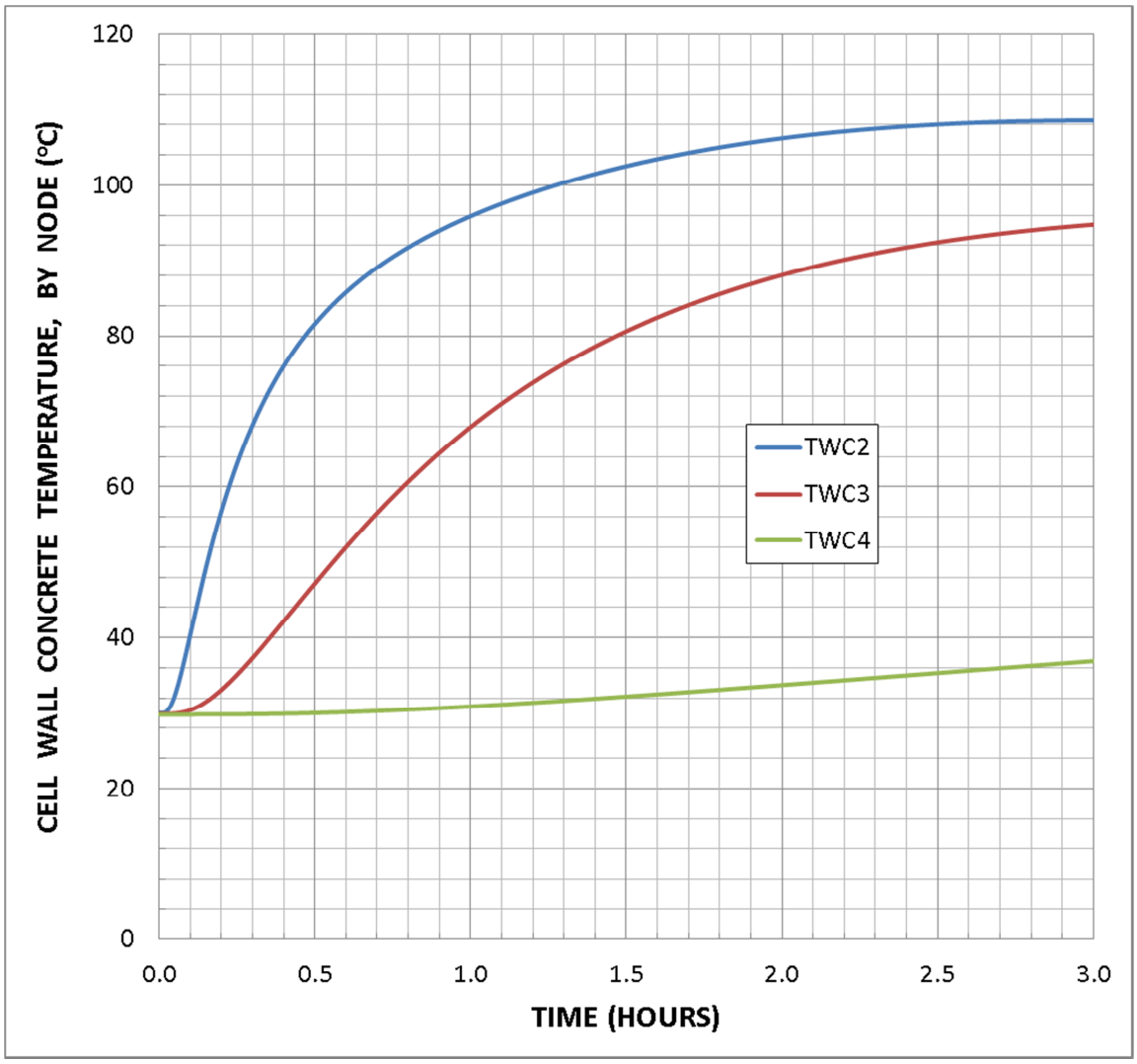

Figure 12. Temperatures Inside of Concrete Wall versus Time for Sodium Pool Fire in Intermediate Sodium Storage Vessel Compartment. The Concrete Wall Thickness Behind the Liner is Divided into Three Nodes of Increasing Thickness.

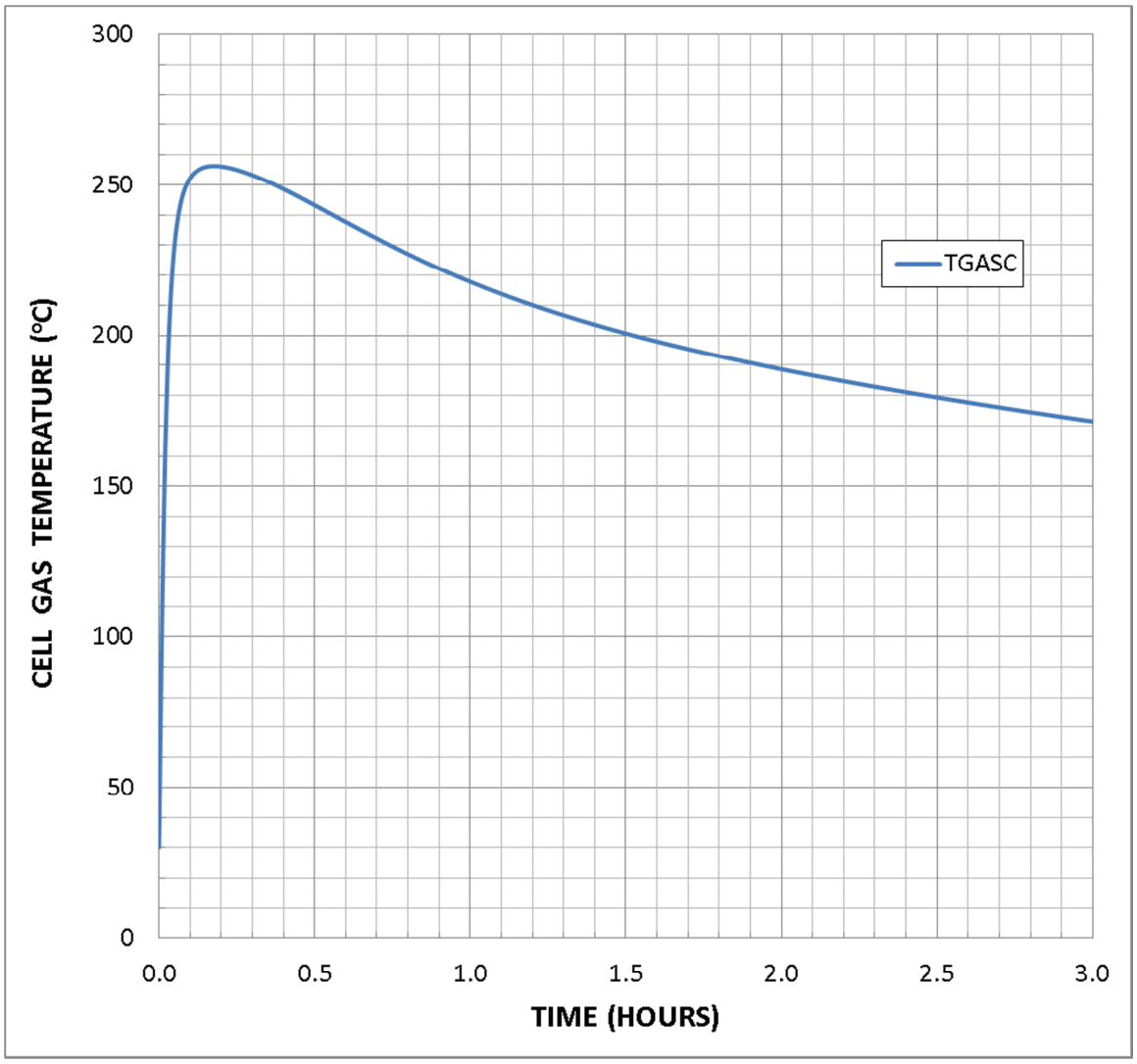

Figure 13. Temperature Inside Compartment Gas Atmosphere versus Time for Sodium Pool Fire in Intermediate Sodium Storage Vessel Compartment.

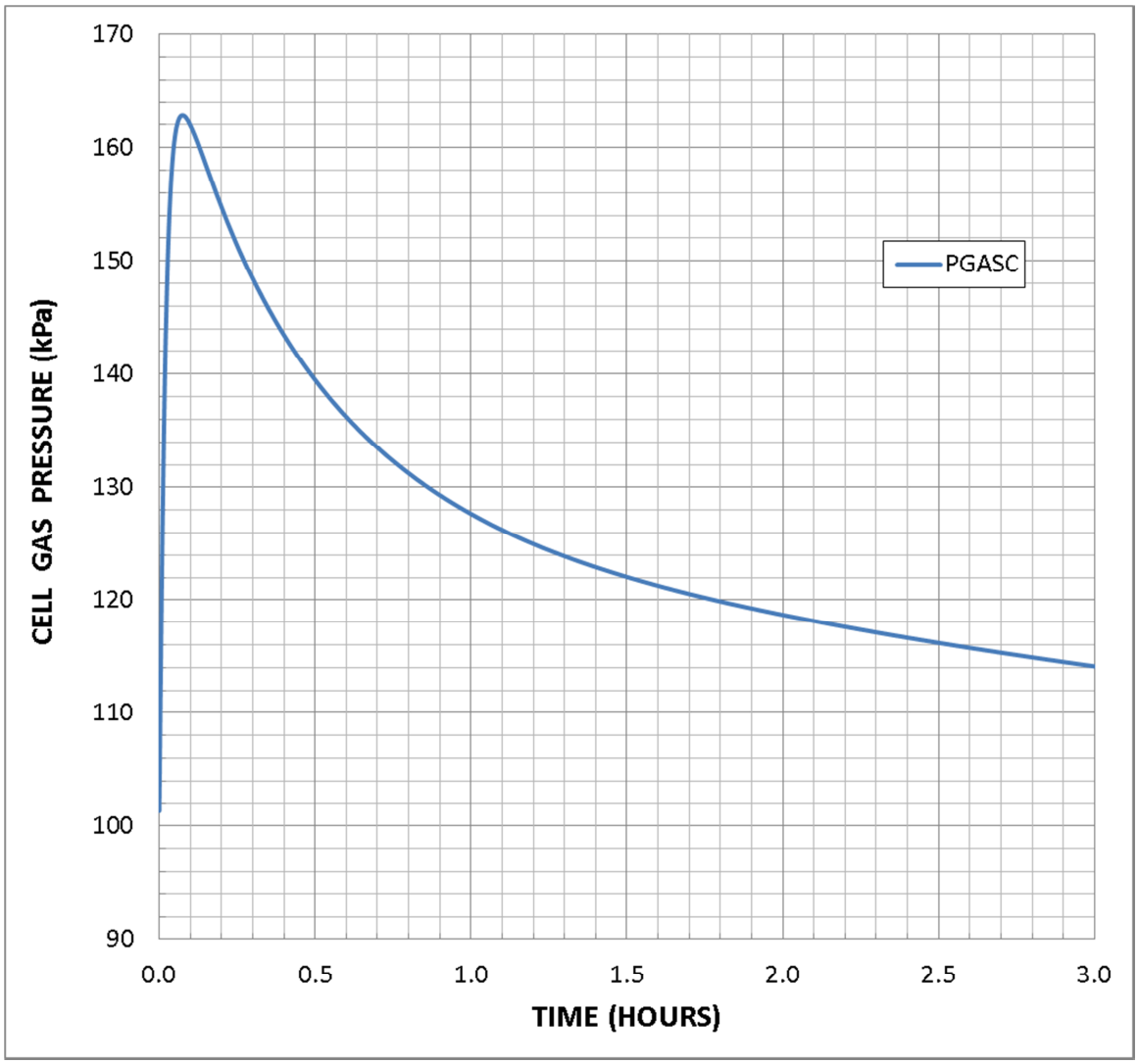

Figure 14. Pressure Inside Compartment Gas Atmosphere versus Time for Sodium Pool Fire in Intermediate Sodium Storage Vessel Compartment.

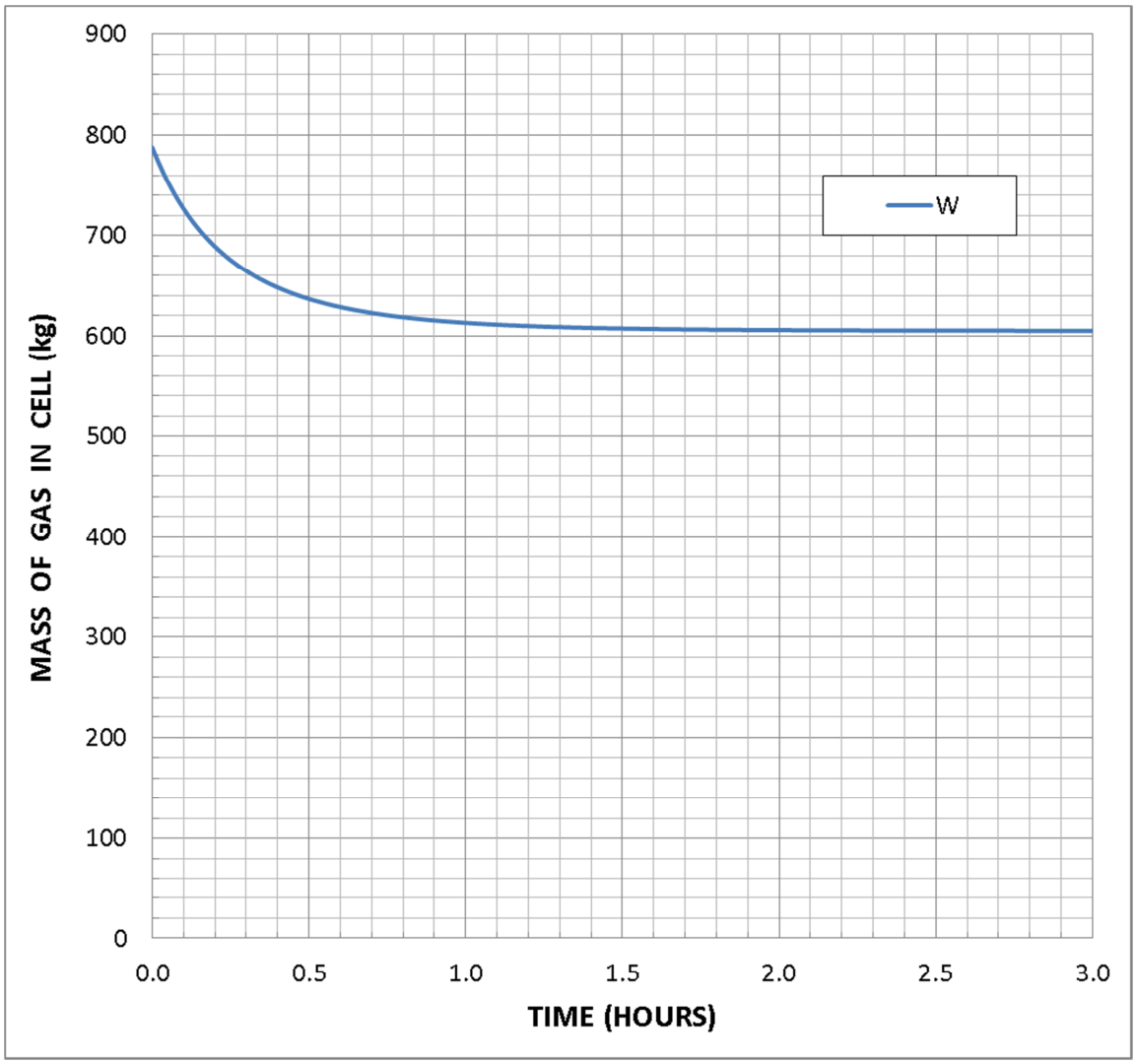

Figure 15. Gas Mass Inside Compartment Gas Atmosphere versus Time for Sodium Pool Fire in Intermediate Sodium Storage Vessel Compartment.

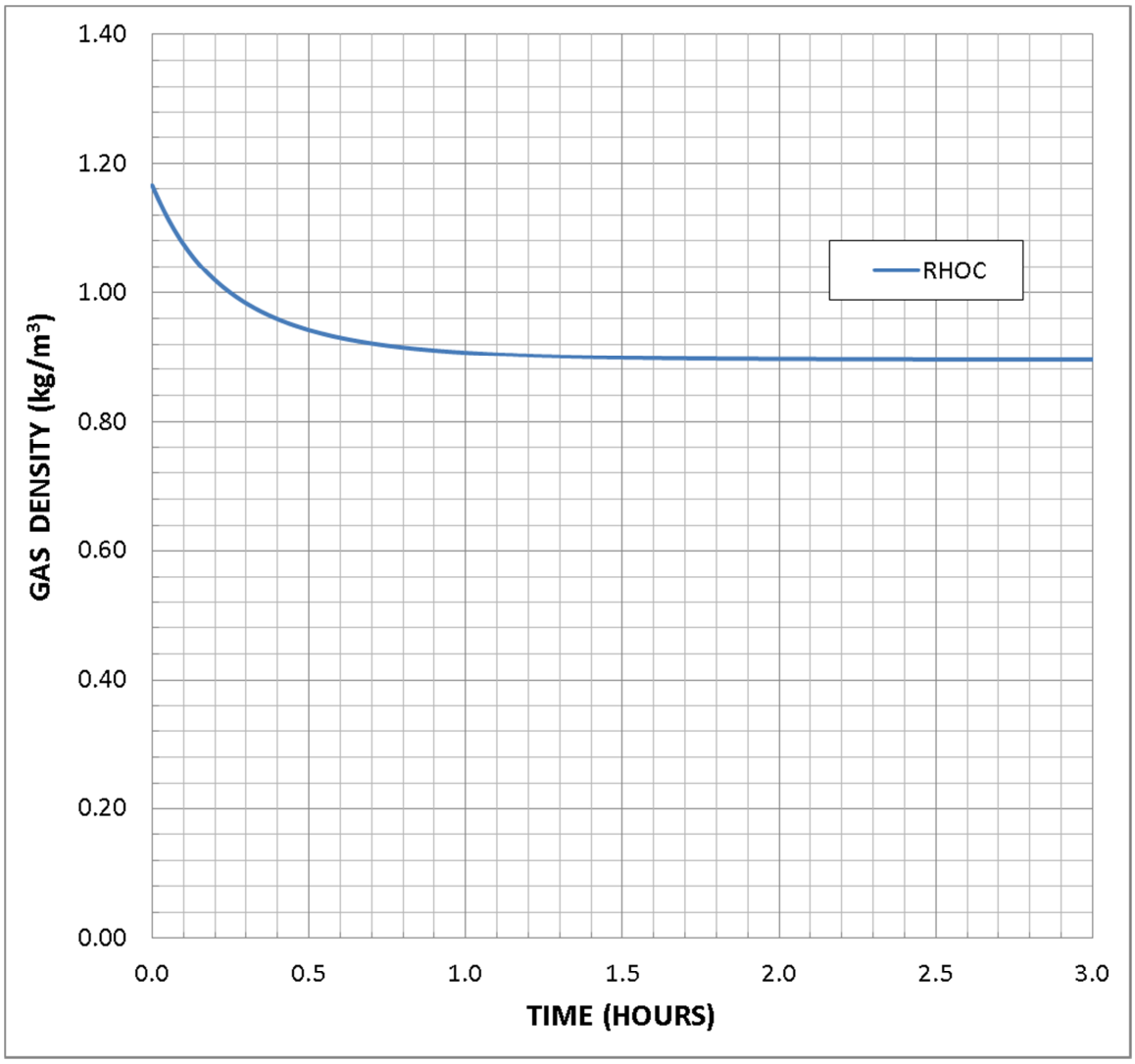

Figure 16. Gas Density Inside Compartment Gas Atmosphere versus Time for Sodium Pool Fire in Intermediate Sodium Storage Vessel Compartment.

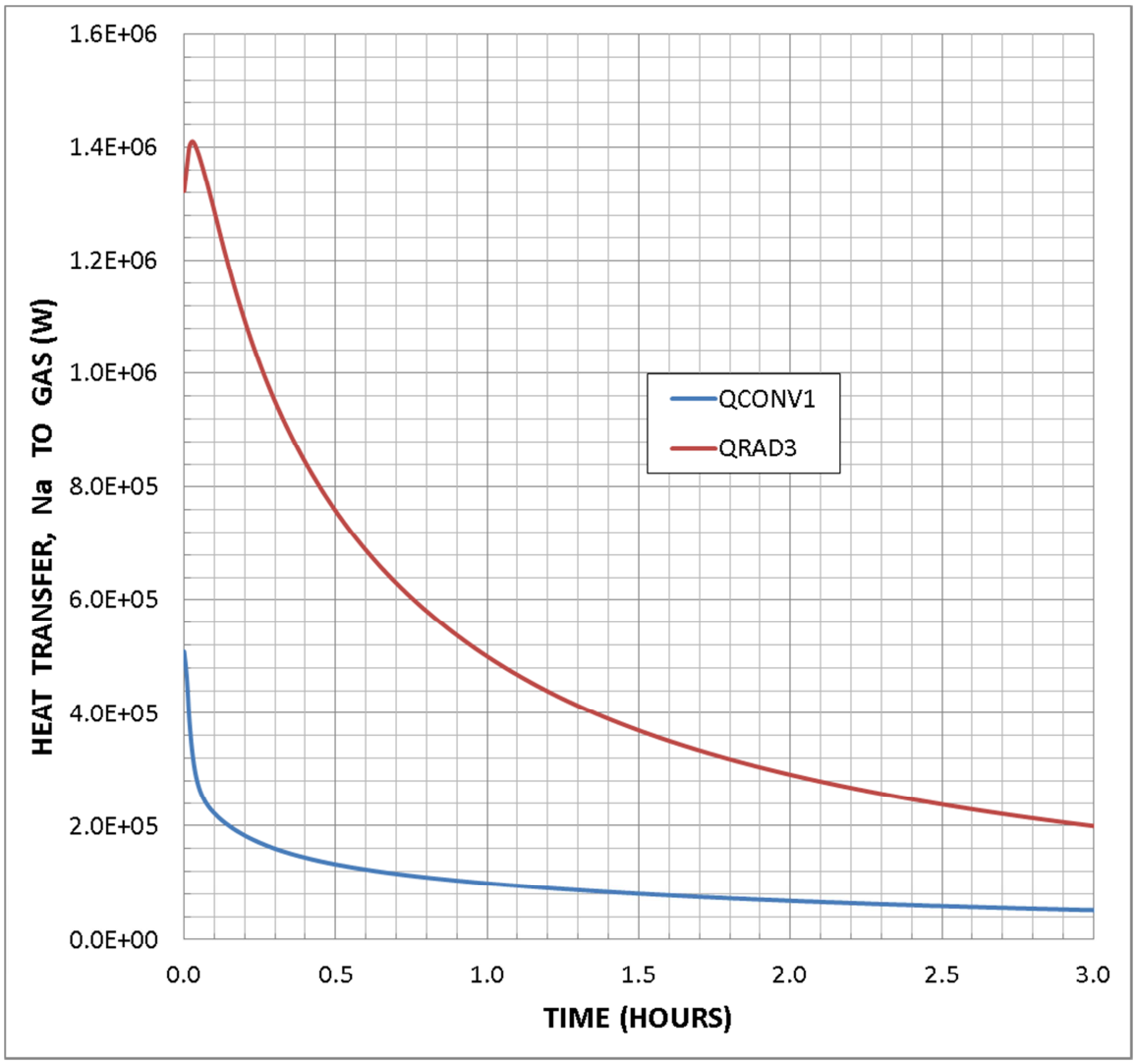

Figure 17. Natural Convection and Thermal Radiation Heat Transfer Rates from Sodium Pool Surface to Compartment Gas Atmosphere versus Time for Sodium Pool Fire in Intermediate Sodium Storage Vessel Compartment.

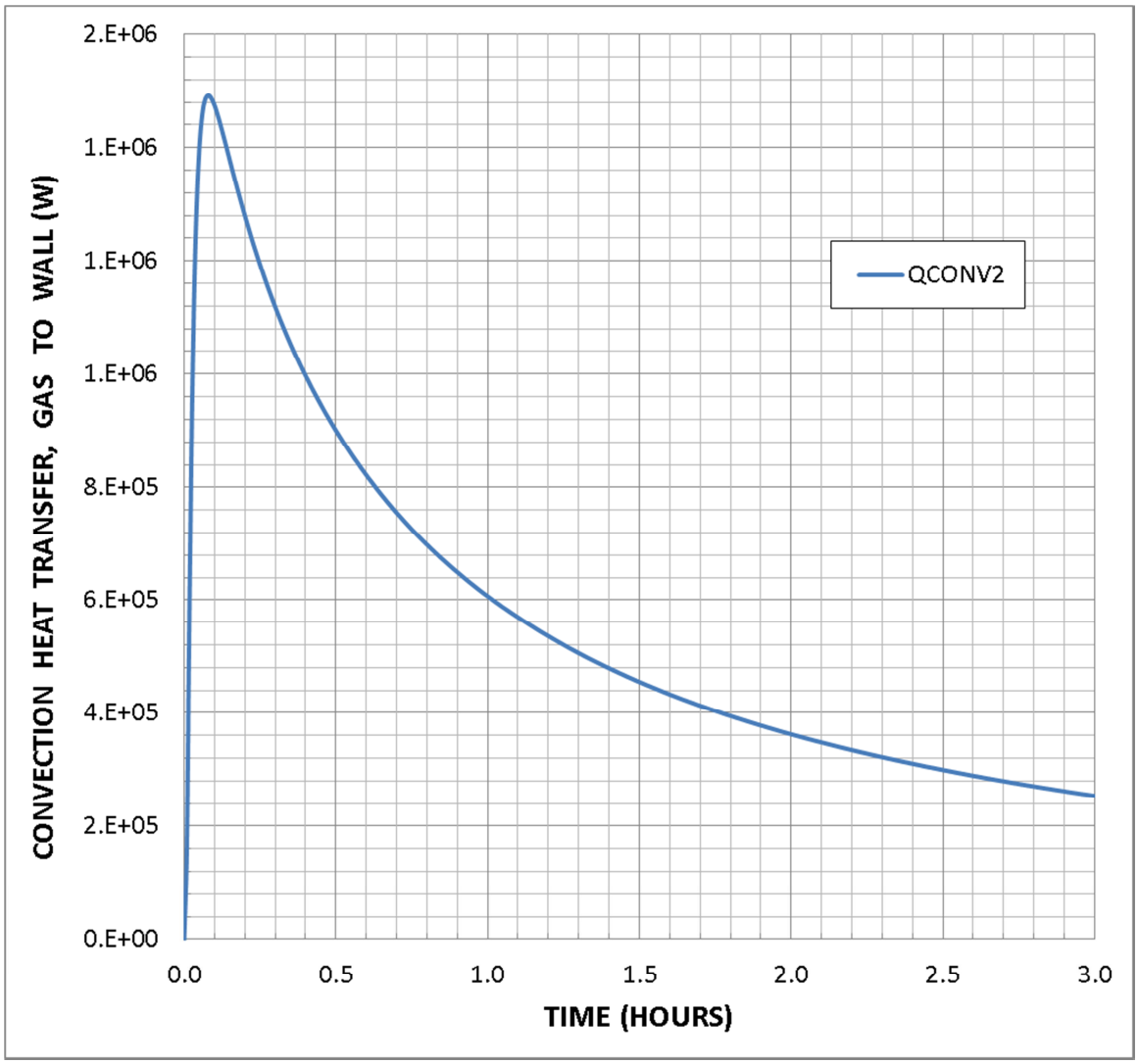

Figure 18. Natural Convection Heat Transfer Rate from Compartment Gas Atmosphere to Wall Liner versus Time for Sodium Pool Fire in Intermediate Sodium Storage Vessel Compartment.

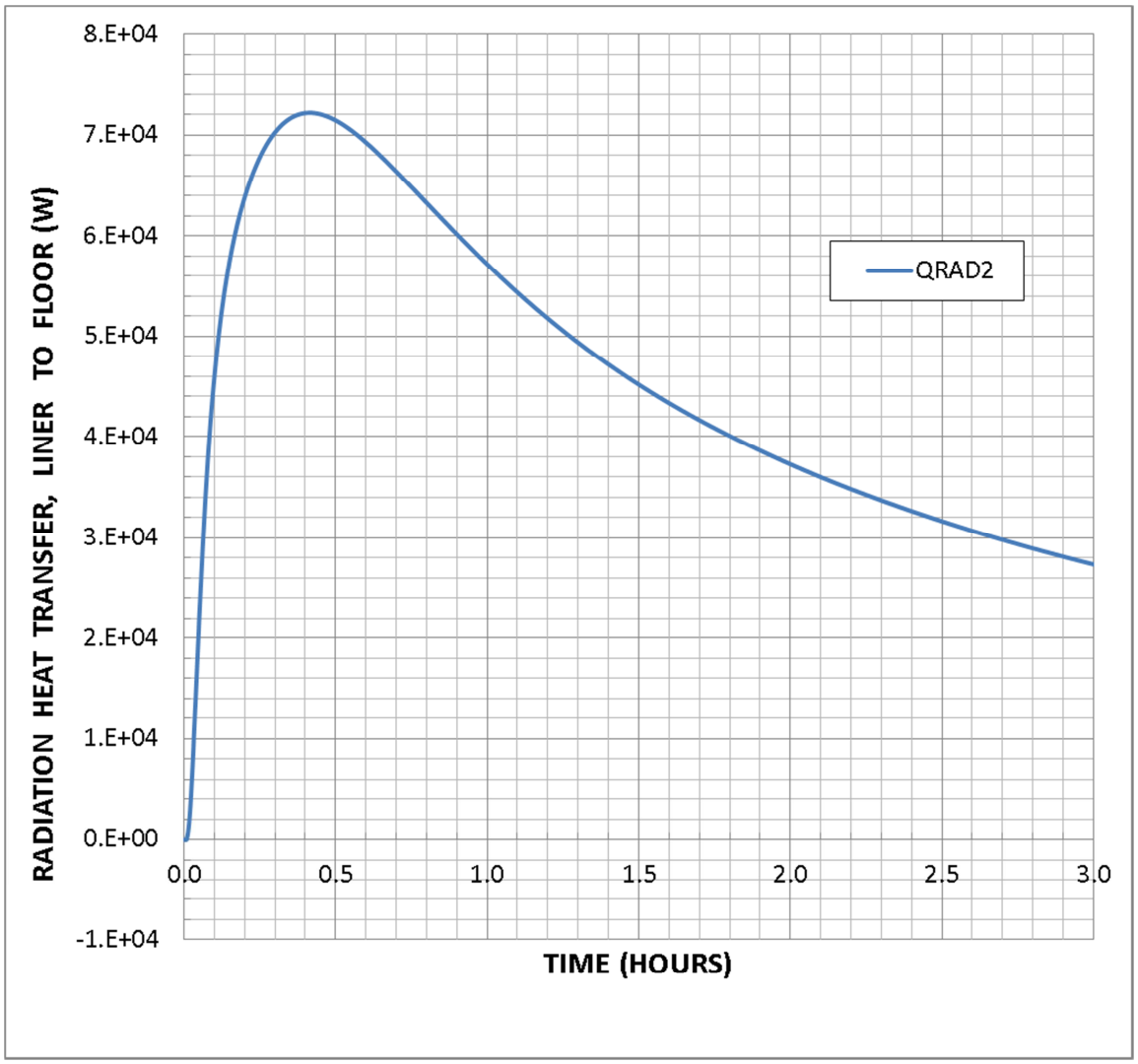

Figure 19. Thermal Radiation Heat Transfer Rate from Steel Floor Liner Across Gap to Floor Concrete versus Time for Sodium Pool Fire in Intermediate Sodium Storage Vessel Compartment.

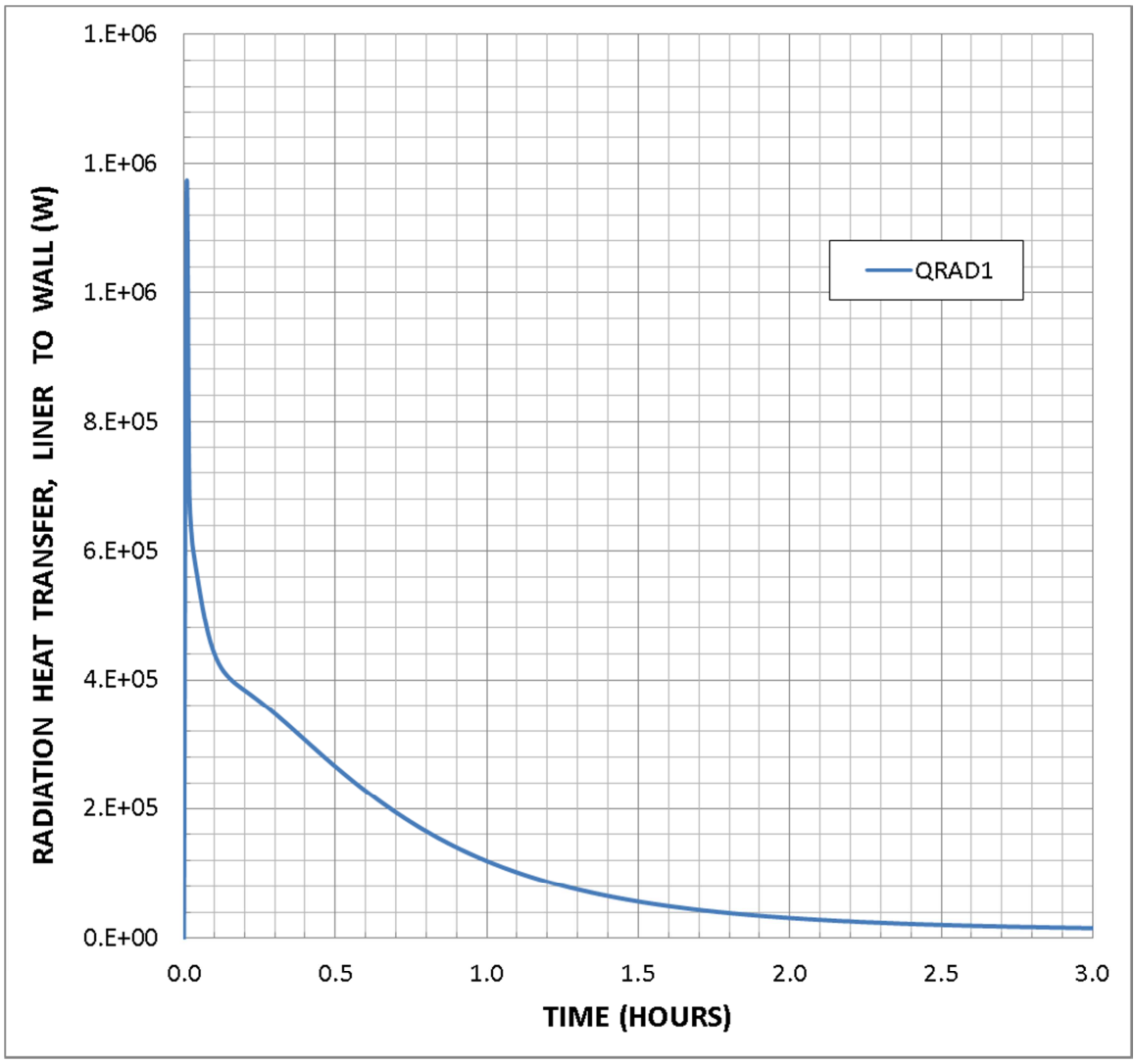

Figure 20. Thermal Radiation Heat Transfer Rate from Steel Wall Liner Across Gap to Wall Concrete versus Time for Sodium Pool Fire in Intermediate Sodium Storage Vessel Compartment.

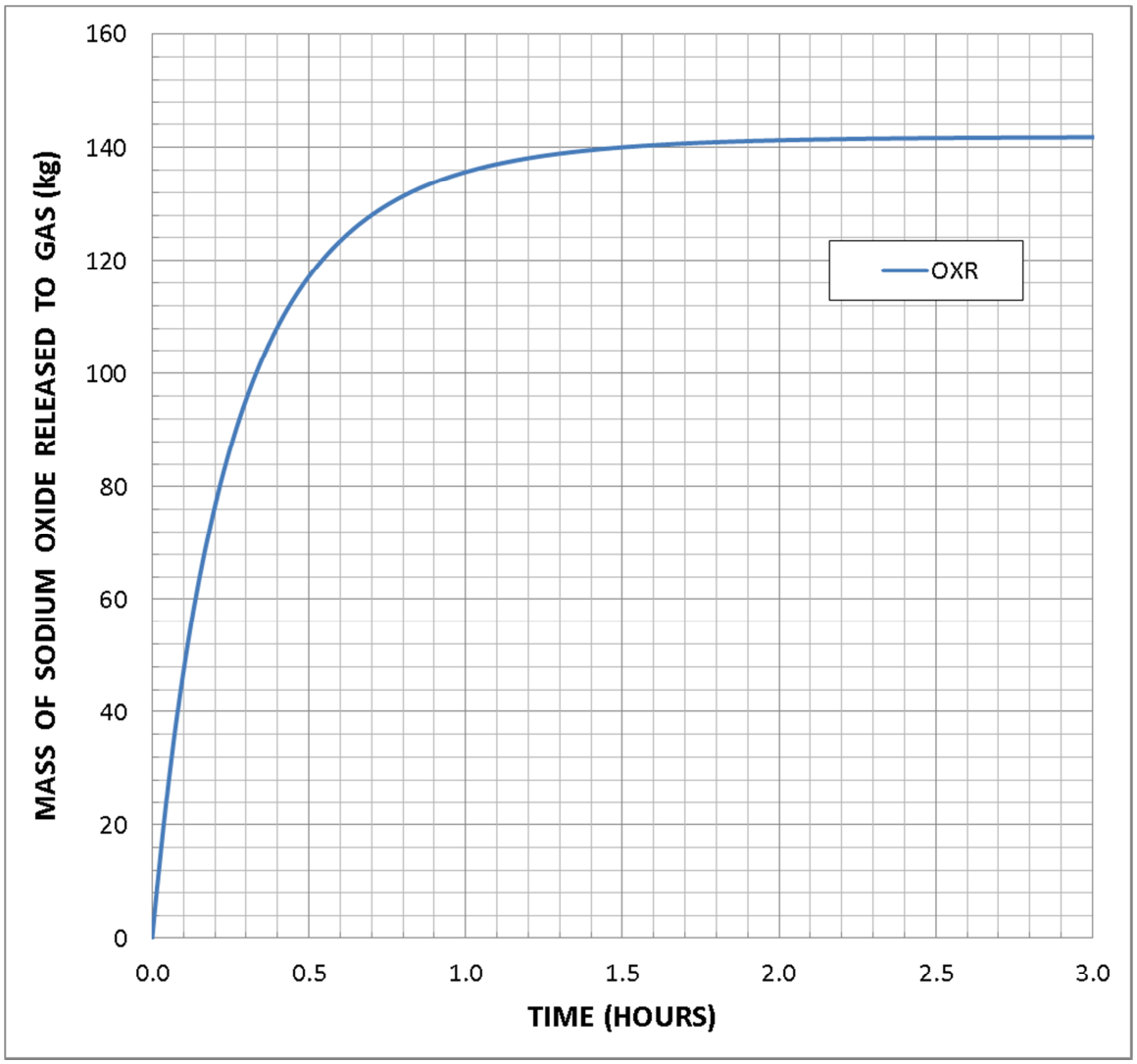

Figure 21. Sodium Oxide Mass Released to Compartment Gas Atmosphere versus Time for Sodium Pool Fire in Intermediate Sodium Storage Vessel Compartment.

In the above calculation, the gaps between the steel liners and the concrete floor and wall are assumed to have a narrow thickness of 0.254 mm (10 mils). The effect of the gap thickness upon the effectiveness of the concrete floor and wall heat sinks was investigated by increasing the gap thickness by an order of magnitude to 2.54 mm (0.1 in). As discussed above, setting the input variables for thermal radiation across the gaps equal to unity might overestimate the effects of thermal radiation across the gaps. Figure 23 through Figure 27 show selected results for the greater gap thickness case. The reduction in the oxygen concentration and the cumulative sodium mass burned versus time (Figure 22 and Figure 23) are virtually identical to those calculated above (Figure 4 and Figure 6). The temperatures at the sodium pool upper surface (Figure 24), inside of the sodium pool (Figure 25), and inside of the steel liner (Figure 26) are somewhat higher than those calculated above (Figure 7, Figure 8, and Figure 9) while the temperatures inside of the concrete floor (Figure 27) are somewhat lower than those calculated above (Figure 10). However, the floor and wall heat sinks are still effective in reducing the sodium pool temperature over time.

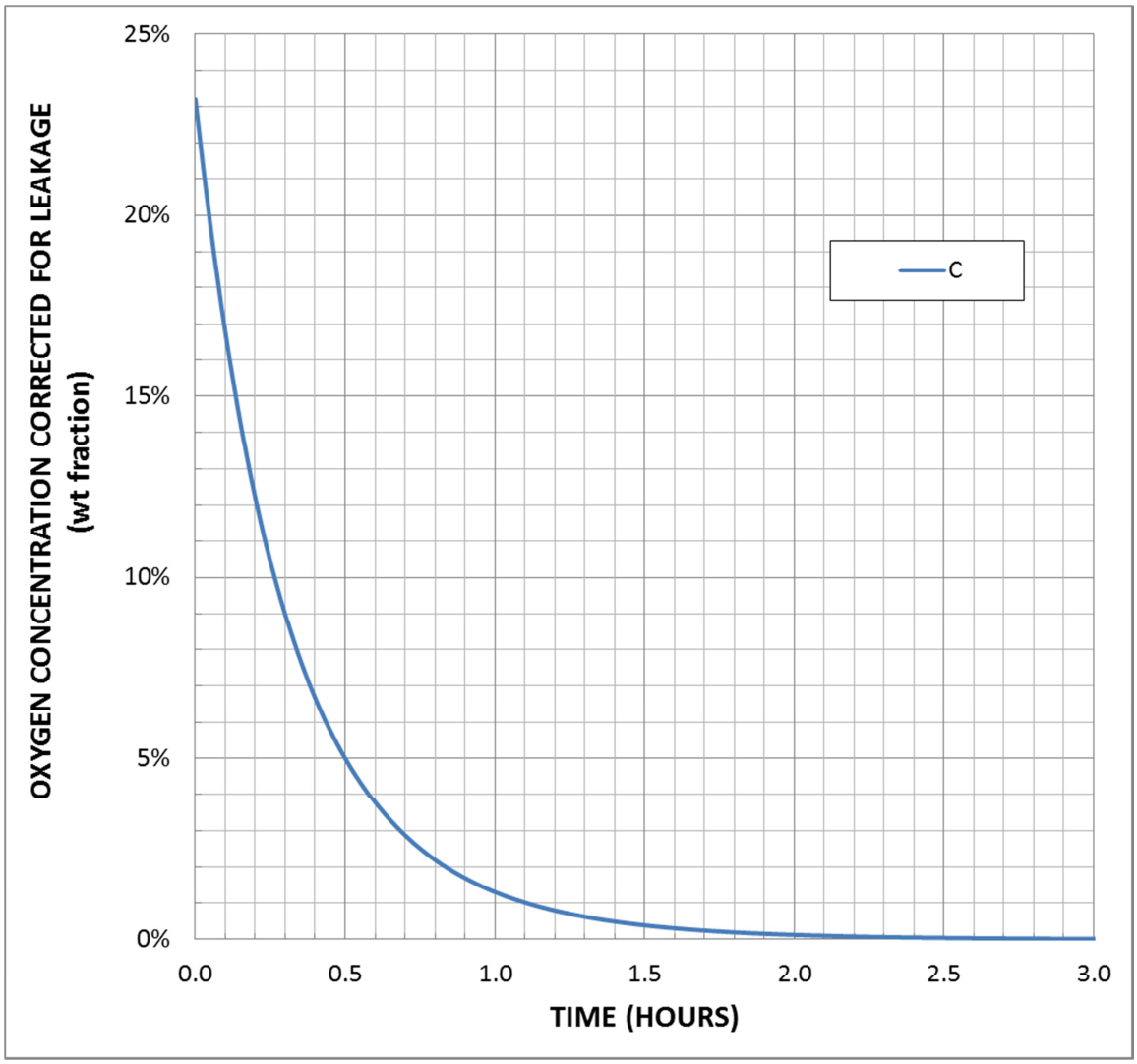

Figure 22. Oxygen Concentration in Compartment Atmosphere versus Time for Sodium Pool Fire in Intermediate Sodium Storage Vessel Compartment with 0.1 inch Gap Thickness between Steel Liners and Concrete.

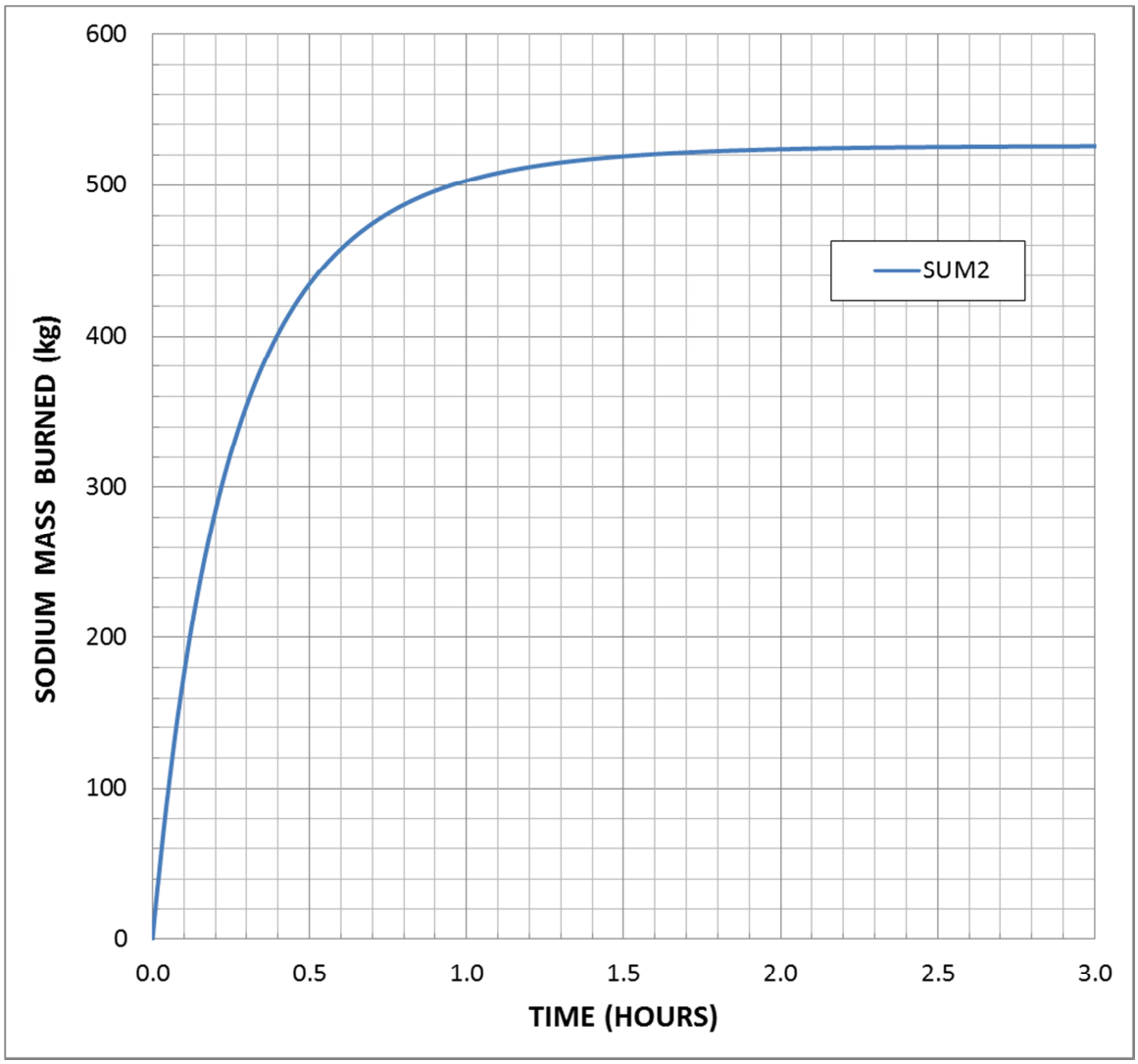

Figure 23. Cumulative Sodium Mass Burned versus Time for Sodium Pool Fire in Intermediate Sodium Storage Vessel Compartment with 0.1 inch Gap Thickness between Steel Liners and Concrete.

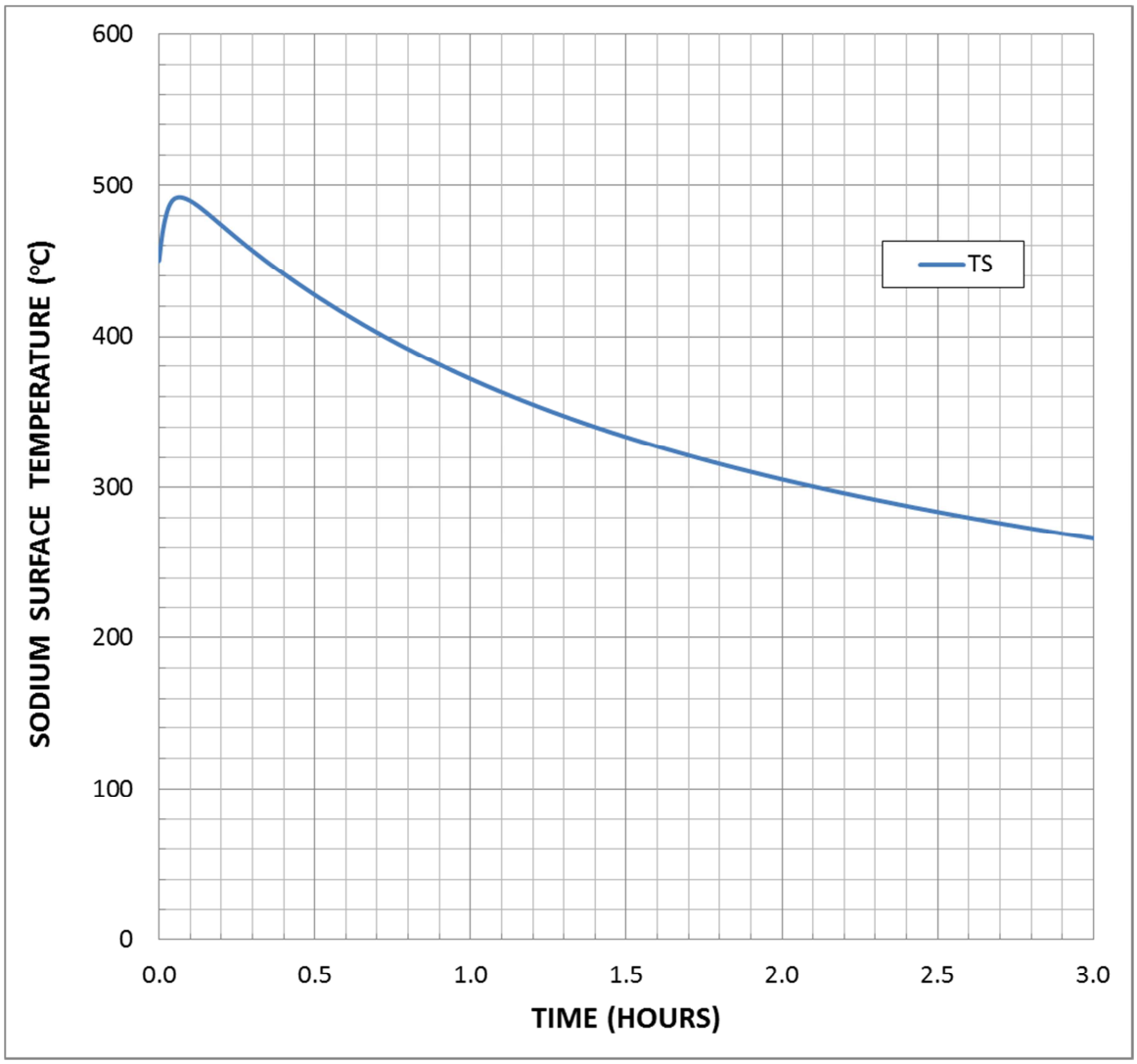

Figure 24. Sodium Upper Surface Node Temperature versus Time for Sodium Pool Fire in Intermediate Sodium Storage Vessel Compartment with 0.1 inch Gap Thickness between Steel Liners and Concrete.

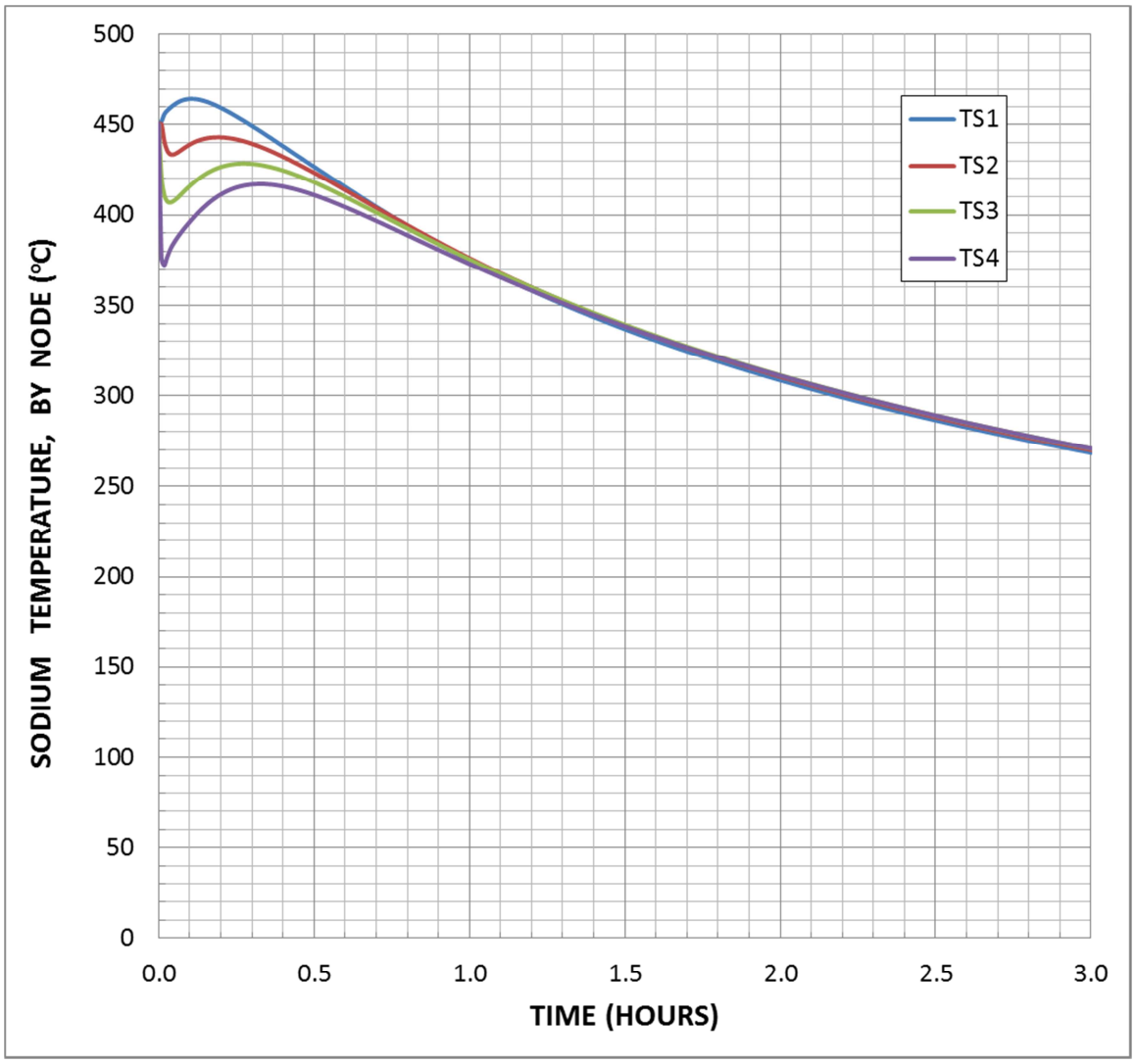

Figure 25. Temperatures of the Four Subsurface Nodes Inside of the Sodium Pool versus Time for Sodium Pool Fire in Intermediate Sodium Storage Vessel Compartment with 0.1 inch Gap Thickness between Steel Liners and Concrete. The Sodium Pool Thickness is Divided into Five Equal Thickness Nodes Consisting of the Surface Node and Four Subsurface Nodes Beneath the Sodium Pool Upper Surface.

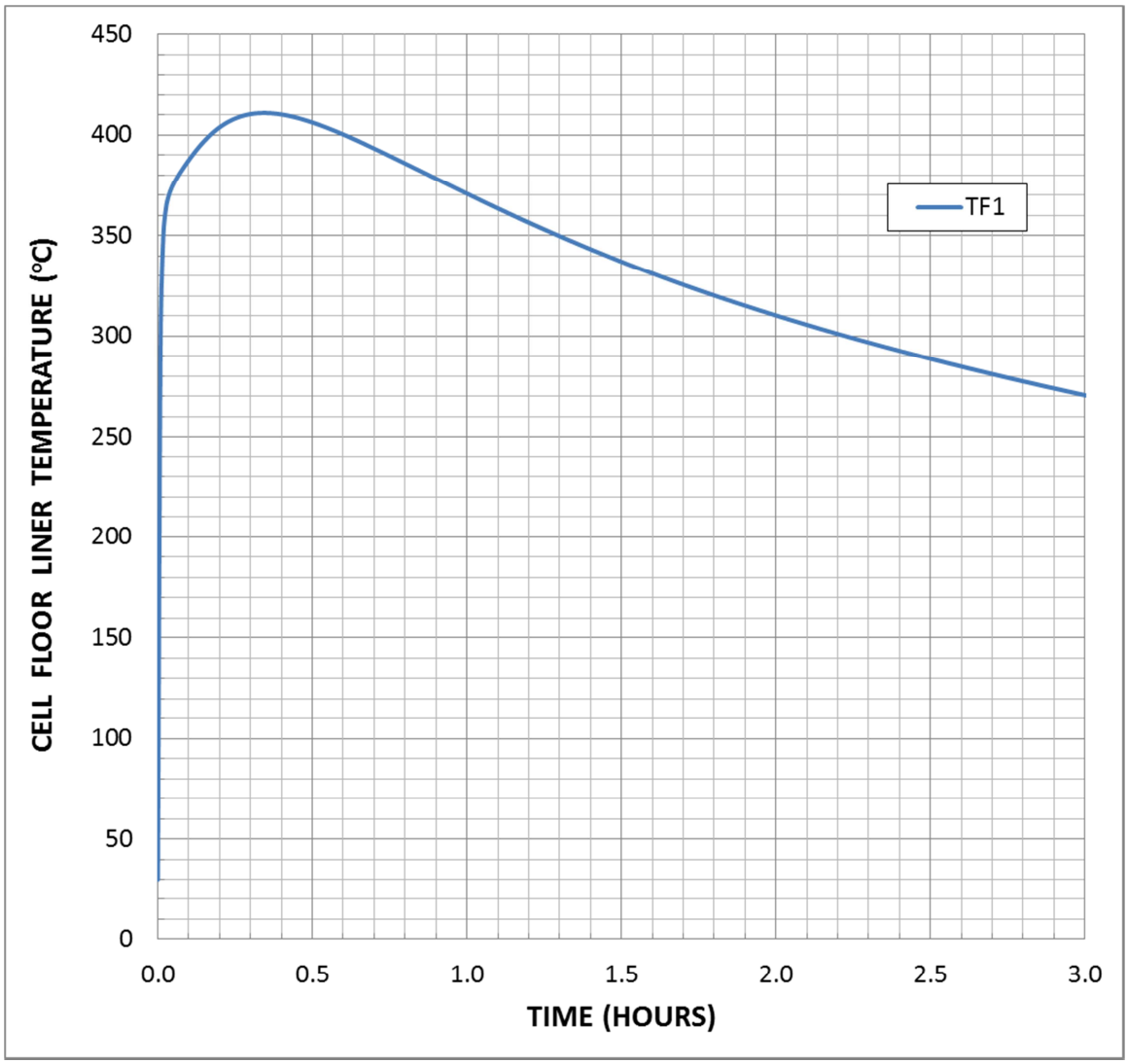

Figure 26. Temperature of Steel Floor Liner versus Time for Sodium Pool Fire in Intermediate Sodium Storage Vessel Compartment with 0.1 inch Gap Thickness between Steel Liners and Concrete.

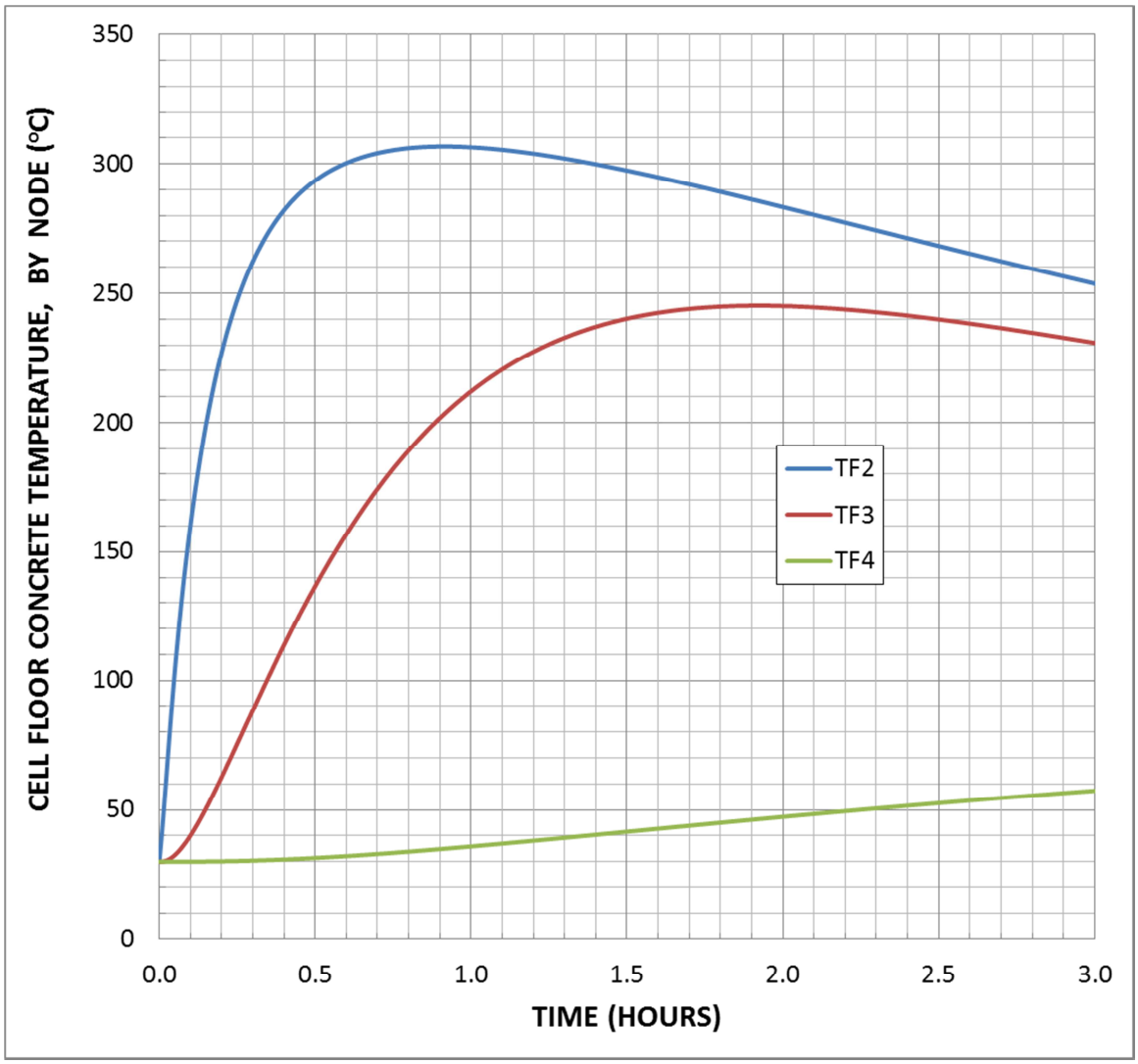

Figure 27. Temperatures Inside of Concrete Floor Nodes versus Time for Sodium Pool Fire in Intermediate Sodium Storage Vessel Compartment with 0.1 inch Gap Thickness between Steel Liners and Concrete. The Concrete Floor Thickness Behind the Liner is Divided into Three Nodes of Increasing Thickness.

The sodium pool temperature decreases with time due to the effects of the compartment heat sinks. It was attempted to illustrate this by defining the code input such that the effects of the heat sinks are set equal to zero. This was found not to be possible without the code running with very small timesteps or not running at all. However, it is possible to minimize the effects of the heat sinks through the input definition. The thermal conductivity of the gas in the steel liner-concrete gaps is set equal to zero and the variables for thermal radiation across the gaps are set equal to zero thereby eliminating heat transfer to the concrete floor and walls from the liners. The specific heat of the gas atmosphere is reduced by a factor of about one thousand reducing the heat capacity of the compartment gas atmosphere. In addition, the walls surface

area is reduced to a very small value to reduce the effects of heat exchange between the gas and wall as well as the heat sink effect of the wall steel liner. The heat sink of the floor steel liner remains; efforts to reduce its effects were met with difficulties in getting the code to run.

Figure 28 and Figure 29 show that the oxygen concentration and cumulative sodium mass burned versus time are virtually identical to those obtained before. Instead of peaking and then decreasing with time due to the heat sink effects, the sodium and steel floor liner temperatures continue to rise with time (Figure 30 through Figure 32). Following consumption of the oxygen in the compartment and reduction in the oxygen concentration reducing the exothermic heat release from reaction of the sodium with oxygen, the temperatures effectively attain a plateau. Presumably, if more oxygen were available, the sodium temperature would continue to rise with time.

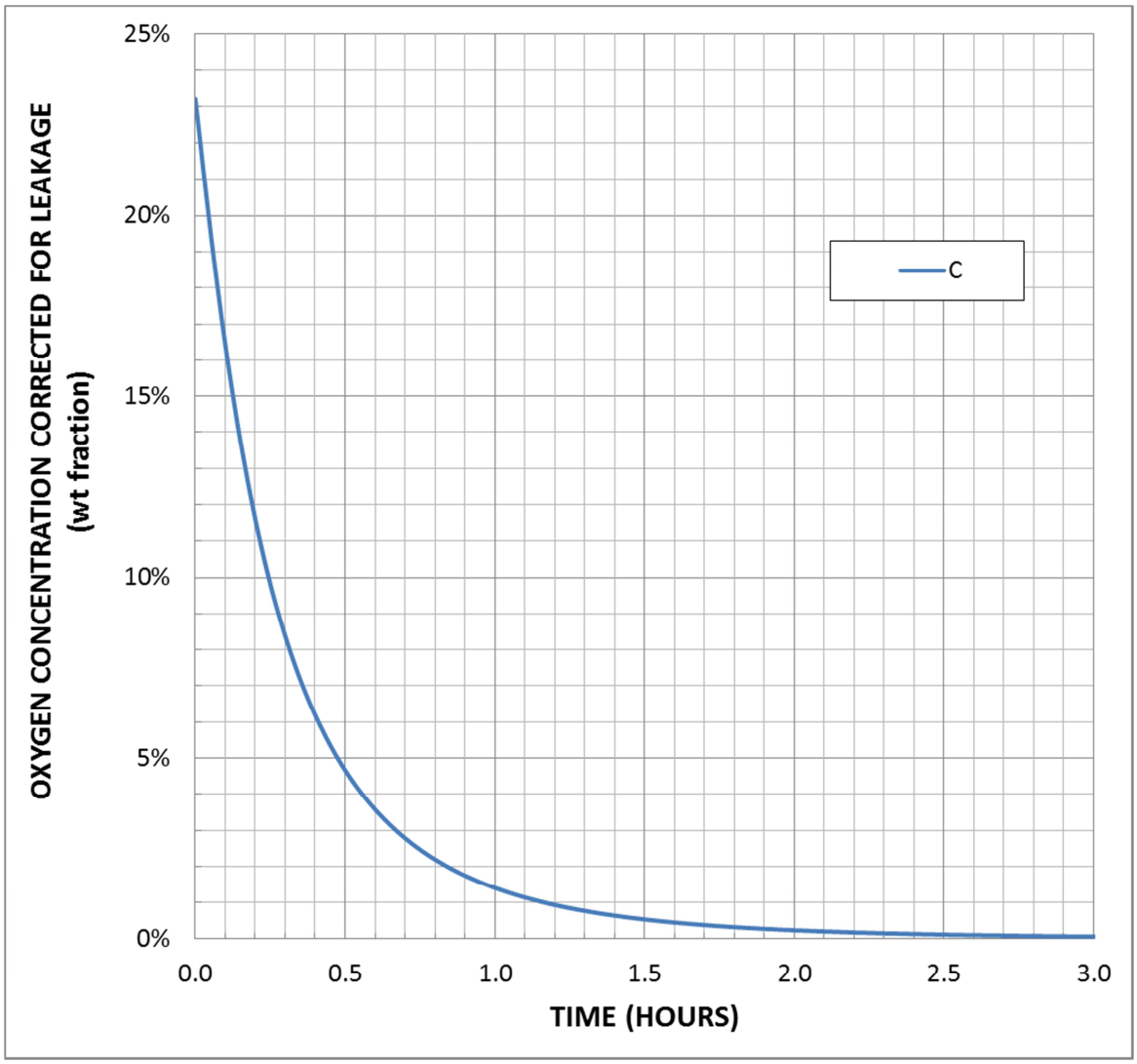

Figure 28. Oxygen Concentration in Compartment Atmosphere versus Time for Sodium Pool Fire in Intermediate Sodium Storage Vessel Compartment with Minimization of Effects of Heat Sinks.

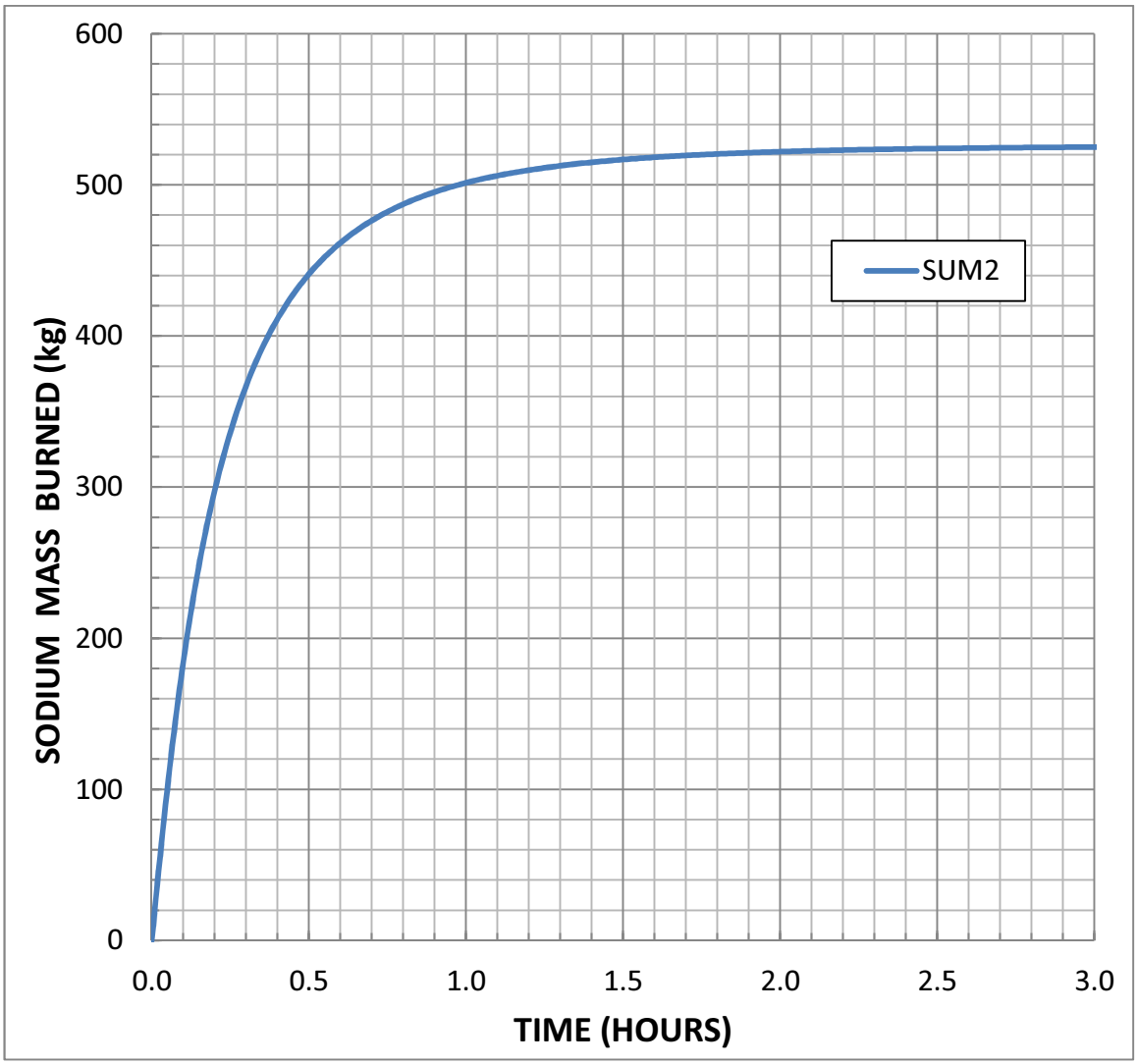

Figure 29. Cumulative Sodium Mass Burned versus Time for Sodium Pool Fire in Intermediate Sodium Storage Vessel Compartment with Minimization of Effects of Heat Sinks.

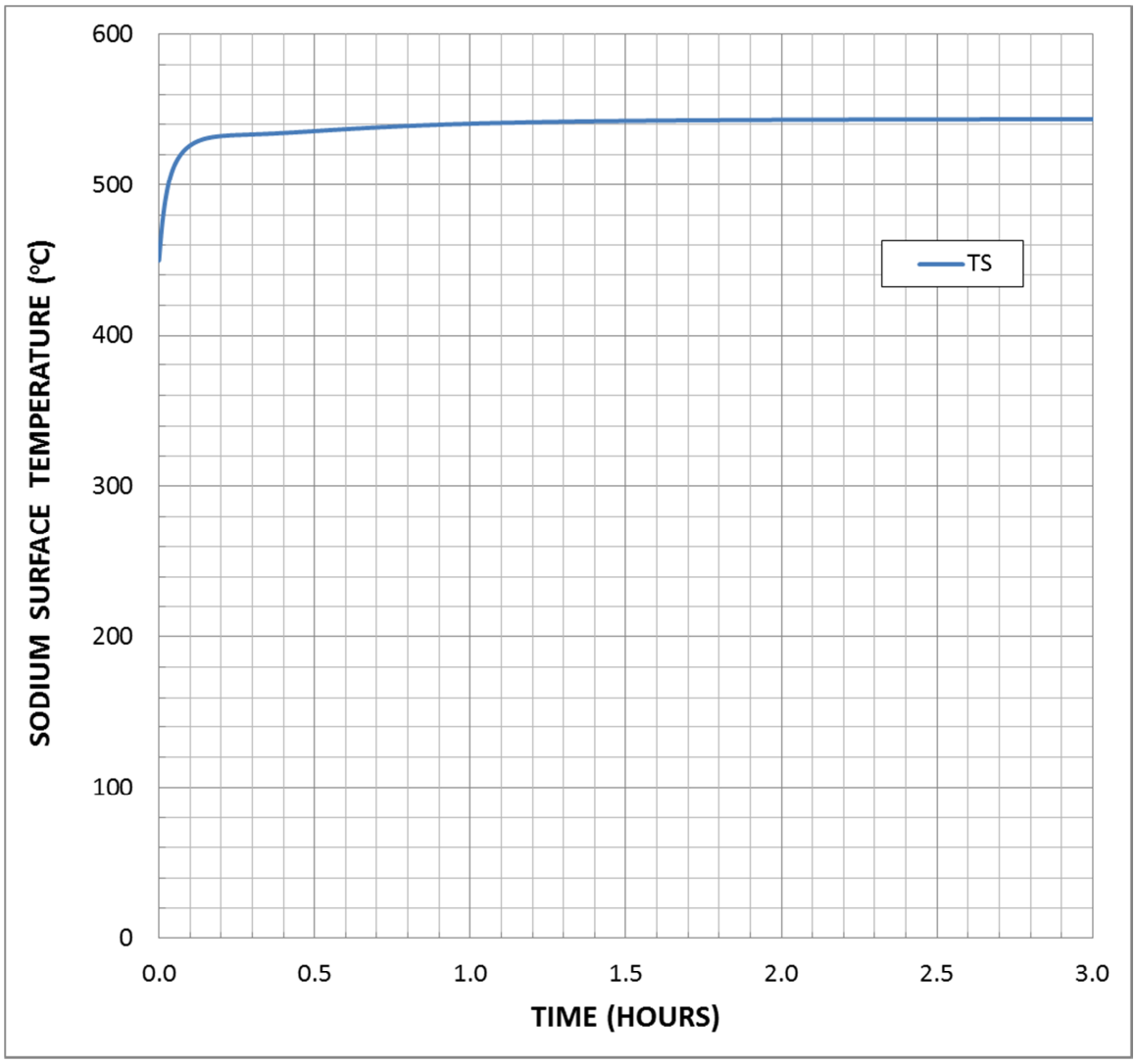

Figure 30. Sodium Upper Surface Node Temperature versus Time for Sodium Pool Fire in Intermediate Sodium Storage Vessel Compartment with Minimization of Effects of Heat Sinks.

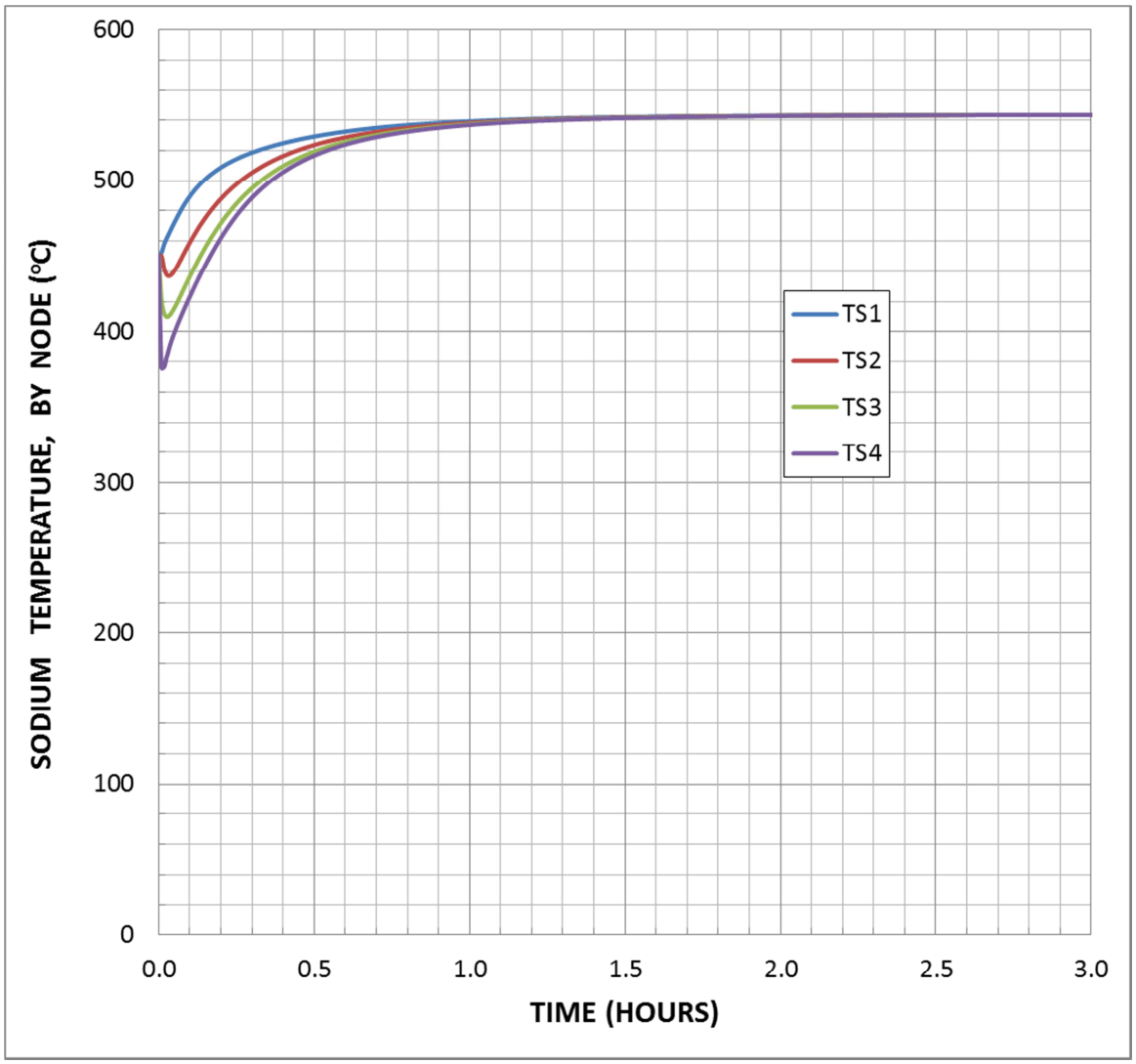

Figure 31. Temperatures of the Four Subsurface Nodes Inside of the Sodium Pool versus Time for Sodium Pool Fire in Intermediate Sodium Storage Vessel Compartment with Minimization of Effects of Heat Sinks. The Sodium Pool Thickness is Divided into Five Equal Thickness Nodes Consisting of the Surface Node and Four Subsurface Nodes Beneath the Sodium Pool Upper Surface.

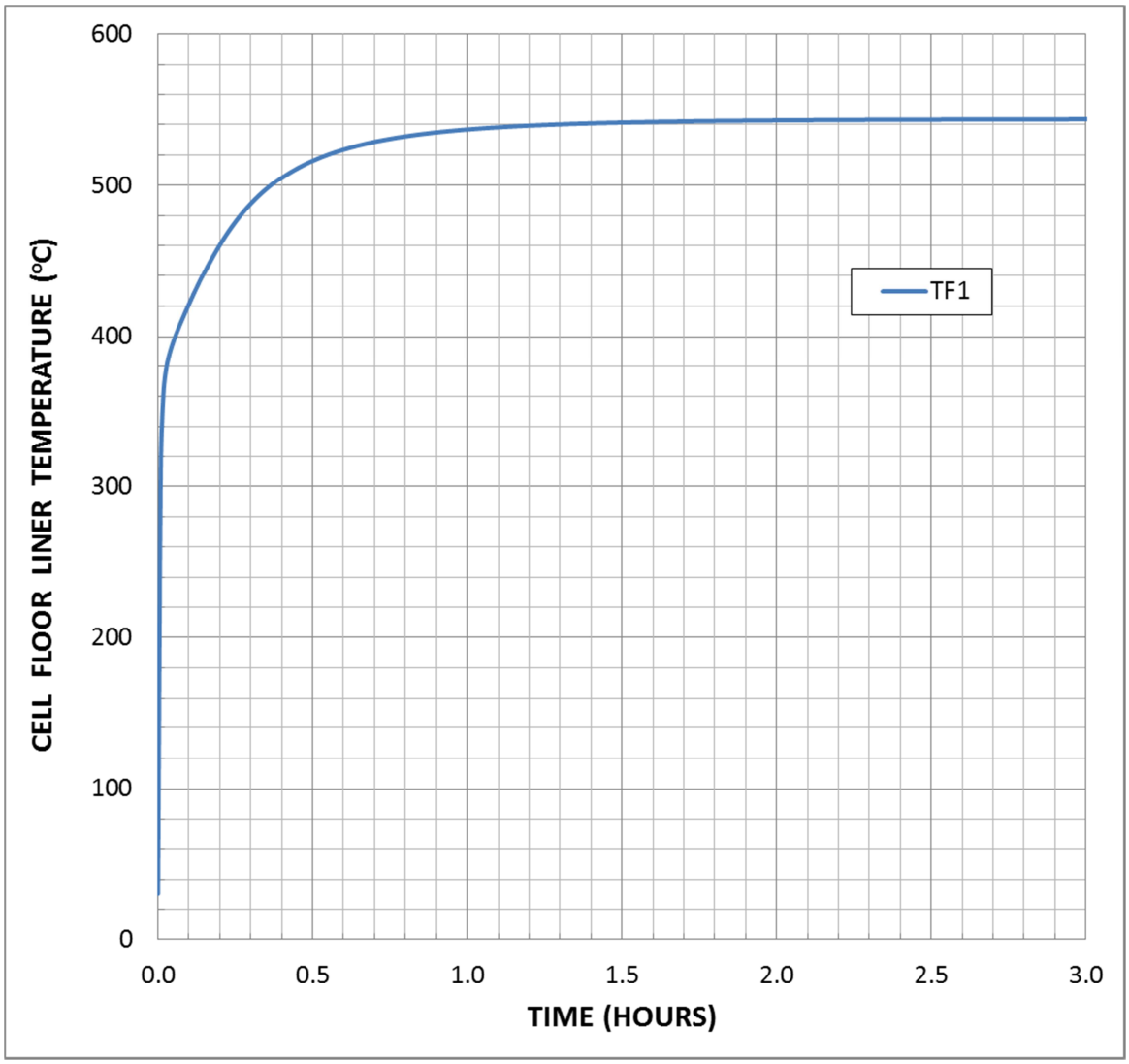

Figure 32. Temperature of Steel Floor Liner versus Time for Sodium Pool Fire in Intermediate Sodium Storage Vessel Compartment with Minimization of Effects of Heat Sinks.

The calculations assume sodium pool burning inside of a closed compartment volume such that fresh air is unable to enter the compartment. If the compartment is not hermetically sealed and there are openings for air, then one can envision a process in which fresh air enters through openings and a portion of the compartment atmosphere escapes through openings. This would give the sodium pool access to additional oxygen such that pool burning could continue. It is of interest to calculate sodium pool burning in such a situation. One could define the compartment volume to be very large such that the oxygen concentration remains virtually unvarying with time. However, such an approach using SOFIRE II ONE CELL would not result in a realistic calculation of the heat up of the actual compartment atmosphere.

7 Summary

The SOFIRE II computer code for the calculation of sodium pool fires has been obtained from the Reactor Safety Information Computational Center and the SOFIRE II ONE CELL version has been implemented at Argonne National Laboratory (ANL). A critical review of literature relevant to sodium pool fires has been carried out with the objectives of understanding sodium pool fire phenomena and how well specific phenomena are modeled or neglected in SOFIRE II. Significant predictions about sodium pool fires can be made on the basis of first principles analyses alone making use of the existing experiment database and knowledge base. In implementing SOFIRE II ONE CELL, minor modifications were necessary to compile and execute the code on a personal computer (PC) and to verify the results of the test case problem. The code was applied to the AFR-100 Sodium-Cooled Fast Reactor (SFR) design to calculate a sodium pool fire following a postulated failure of the sodium storage vessel of one of the four intermediate sodium heat transport circuits and the subsequent release of sodium onto the floor of the steel-lined compartment in which the sodium storage vessel is located. SOFIRE II calculates that only a small fraction of the released sodium burns due to the rapid consumption of the available oxygen inside of the closed compartment. The preliminary results demonstrate the effects of the heat sinks provided by the compartment floor, walls, and ceiling in reducing the temperature of the sodium pool with time.

Acknowledgements

Argonne National Laboratory's work was supported by the U. S. Department of Energy Advanced Reactor Concepts (ARC) Program under Prime Contract No. DE-AC02-06CH11357 between the U.S. Department of Energy and UChicago Argonne, LLC. The work presented here was carried out under the Fast Spectrum Reactor area of the ARC Program. The authors are grateful to Chris Grandy (ANL), the Technical Area Lead, Bob Hill (ANL/NE), the National Technical Director, and Jason Tokey (U.S. DOE), the Headquarters Program Manager for the Advanced Reactor Concepts (ARC) Program.

References

1. P. Beiriger, J. Hopenfeld, M. Silberberg, R. P. Johnson, L. Baurmash, and R. L. Koontz, "SOFIRE II User Report," AI-AEC-13055, LMFBR SAFETY, UC-79p, Atomics International Division, Rockwell International, Canoga Park, CA March 30, 1973.
2. R. N. Newman and J. F. B. Payne, "Fundamental Studies of the Mechanism of Sodium Combustion," Proceedings of the International Conference on Liquid Metal Technology in Energy Production, Champion, PA, November 1976, CONF-760503-p2, Distribution Category UC-79a, U.S. Government Printing Office, 1977.
3. R. N. Newman and J. F. B. Payne, "The Burning Rates of Sodium Pool Fires," Combustion and Flame, Vol. 33, pp. 291-297, 1978.
4. R. N. Newman, "The Role of Carbon Dioxide in the Combustion of Sodium in Air," Proceedings of the L.M.F.B.R. Safety Topical Meeting, Lyon-Ecully France, July 19-23, 1982, Volume III, pp. III-3-III-11, SFEN, 1982.
5. R. N. Newman, "The Ignition and Burning Behavior of Sodium Metal in Air," Progress in Nuclear Energy, Vol. 12, No. 2, pp. 119-147, 1983.
6. S. Globe and D. Dropkin, "Natural-Convection Heat Transfer in Liquids Confined by Two Horizontal Plates and Heated from Below," Transactions of the ASME, Journal of Heat Transfer, Vol. 81, pp. 24-28, February 1959.
7. M. Fishenden and O. A. Saunders, An Introduction to Heat Transfer, Oxford University Press, London, 1950.
8. S. W. Churchill and H. H. S. Chu, "Correlating Equations for Laminar and Turbulent Free Convection from a Vertical Plate," International Journal of Heat and Mass Transfer, Vol. 18, pp. 1323-1329, 1975.
9. D. A. Saville and S. W. Churchill, "Simultaneous Heat and Mass Transfer in Free Convection Boundary Layers," AIChE Journal, Vol. 16, No. 3, pp. 268-273, March 1970.
10. M. Al-Arabi and M. K. El-Riedy, "Natural Convection Heat Transfer from Isothermal Horizontal Plates of Different Shapes," International Journal of Heat and Mass Transfer, Vol. 19, pp. 1399-1404, 1976.
11. M. Nishimura, H. Kamide, S. Otake, and K-i Sugiyama, "Features of Dendritic Oxide during Sodium Combustion," Journal of Nuclear Science and Technology, Vol. 48, No. 12, pp. 1420-1427, 2011.
12. M. Nishimura, K. Nagai, T. Onojima, J-i Saito, K. Ara, and K-i Sugiyama, "The Sodium Oxidation Reaction and Suppression Effect of Sodium with Suspended Nanoparticles – Growth Behavior of Dendritic Oxide during Oxidation," Journal of Nuclear Science and Technology, Vol. 49, No. 1, pp. 71-77, 2012.

13. Journal of Physical and Chemical Reference Data Monograph No. 9 NIST-JANAF Thermochemical Tables Fourth Edition Part II, Cr-Zr, American Chemical Society and American Institute of Physics for the National Institute of Standards and Technology, Woodbury, New York, 1998.
14. H. M. Kottowski, "Survey on Sodium Chemistry," Safety Problems Related to Sodium Handling in Liquid Metal Fast Breeder Reactors and Large Test Facilities, Lectures from a Course Held at the Joint Research Centre, Ispra (Italy), November 12-14, 1980, Ed. H. M. Kottowski, pp. 3-37, Harwood Academic Publishers, France, 1981.
15. S. Jordan, "Aerosols Released from Burning Sodium," Safety Problems Related to Sodium Handling in Liquid Metal Fast Breeder Reactors and Large Test Facilities, Lectures from a Course Held at the Joint Research Centre, Ispra (Italy), November 12-14, 1980, Ed. H. M. Kottowski, pp. 177-198, Harwood Academic Publishers, France, 1981.
16. CRC Handbook of Chemistry and Physics 1977-1978 58th Edition, Ed. R. C. Weast, CRC Press Inc., Cleveland, 1977.
17. A. Yamaguchi and Y. Tajima, "Validation Study of Computer Code SPHINCS for Sodium Fire Safety Evaluation of Fast Reactor," Nuclear Engineering and Design, Vol. 219, pp. 19-34, 2003.
18. O. Miyake, S. Miyahara, S. Ohno, and Y. Himeno, "Sodium Pool Combustion Codes for Evaluation of Fast Breeder Reactor Safety," Journal of Nuclear Science and Technology, Vol. 28, No. 2, pp. 107-121, February 1991.
19. K. Marimuthu, "Sodium Fire Code SFIRE1C for Pool Fire Characteristics," Journal of Nuclear Science and Technology, Vol. 33, No. 10, pp. 787-791, October 1996.
20. W. Schütz and H. Sauter, "Experimental Determination of Sodium Evaporation Rates," Nuclear Science and Engineering, Vol. 80, pp. 667-672, 1982.

Nuclear Engineering Division
Argonne National Laboratory
9700 South Cass Avenue, Bldg. #208
Argonne, IL 60439

www.anl.gov

Argonne National Laboratory is a U.S. Department of Energy laboratory managed by UChicago Argonne, LLC